A novel approach to transport through correlated quantum dots

C. Karrasch,[1] T. Enss,[2] and V. Meden[1]

[1] *Institut für Theoretische Physik, Universität Göttingen, Friedrich-Hund-Platz 1, D-37077 Göttingen, Germany*

[2] *Istituto Nazionale di Fisica della Materia–SMC–CNR and Dipartimento di Fisica, Università di Roma "La Sapienza", Piazzale Aldo Moro 2, I-00185 Roma, Italy*

We investigate the effect of local Coulomb correlations on electronic transport through a variety of coupled quantum dot systems connected to Fermi liquid leads. We use a newly developed functional renormalization group scheme to compute the gate voltage dependence of the linear conductance, the transmission phase, and the dot occupancies. A detailed derivation of the flow equations for the dot level positions, the inter-dot hybridizations, and the effective interaction is presented. For specific setups and parameter sets we compare the results to existing accurate numerical renormalization group data. This shows that our approach covers the essential physics and is quantitatively correct up to fairly large Coulomb interactions while being much faster, very flexible, and simple to implement. We then demonstrate the power of our method to uncover interesting new physics. In several dots coupled in series the combined effect of correlations and asymmetry leads to a vanishing of transmission resonances. In contrast, for a parallel double-dot we find parameter regimes in which the two-particle interaction generates additional resonances.

PACS numbers: 73.63.-b, 73.63.Kv, 73.23.Hk

I. INTRODUCTION

Electronic transport through multi-level quantum dots and several coupled dots is currently of great experimental and theoretical interest due to the possible application of such systems in interferometers and for charge- and spin-based quantum information processing.[1,2,3,4,5,6,7,8,9,10,11,12] The smallness of the mesoscopically confined electron droplet—the quantum dot—leads to fairly large energy level spacings and at sufficiently small temperatures T only a few levels must be considered. The physics is strongly affected by charging effects[1] (Coulomb blockade) and local Coulomb correlations, e.g. leading to the Kondo effect.[13,14,15,16,17,18]

We here present a new method to describe the low-temperature transport through both a single multi-level dot and several coupled dots. To keep the notation short when referring to both situations in the following we denote the dot(s) as the mesoscopic system. We investigate the linear response conductance G through the setup as a function of a gate voltage V_g that shifts the energy levels. The connection between the mesoscopic system and the leads (the reservoirs) is modeled by low-transmission tunneling barriers.

The transport through a single-level dot with spin degeneracy (see Fig. 1 A) is well understood. For simplicity we only consider equal couplings to the left and right lead. At small T and for noninteracting dot electrons $G(V_g)$ shows a Lorentzian resonance of unitary height $2e^2/h$ placed roughly at the energy of the single-particle level of the dot. The full width 2Γ of the resonance sets an energy scale Γ that is associated with the strength of the tunneling barriers. Including a Coulomb interaction U between the spin up and down dot electrons the line shape is substantially altered as can be seen from the exact $T = 0$ Bethe ansatz solution.[19] For increasing U/Γ it is gradually transformed into a box-shaped resonance of unitary heights with a plateau of width U and a sharp decrease of G to the left and right of it.[14,15,20,21] For gate voltages within the plateau the dot is half-filled implying a local spin-1/2 degree of freedom on the dot. Thus, the Kondo effect[13] leads to resonant transport throughout this Kondo regime. A linear chain of a few coupled single-level dots (see Fig. 1 B) presents a simple extension of the single-dot case and was studied recently.[22,23,24] This system can equally be viewed as a short Hubbard chain.

In more complex cases in which electrons can pass the mesoscopic system following different paths, not only correlations but also quantum interference plays an important role, leading e.g. to the Fano[25] effect. Realizations of such a situation that have been studied theoretically are: i) A single dot coupled to two leads that are in addition coupled by a direct transmission channel (Aharonov-Bohm interferometer with an embedded dot) as sketched in Fig. 1 C.[26] ii) A system of two dots, one directly connected to the two leads and the other side-coupled to the first one[27,28,29] shown in Fig. 1 D. iii) Parallel double dots coupled to common leads[30,31,32,33] (see Fig. 1 E) that have also been realized experimentally.[4,5,6,7,8,10,11] The combined effect of multi-path interference through several nearly degenerate levels of a single dot and correlations is discussed as one of the possible reasons for the puzzling behavior of the transmission phase measured in an Aharonov-Bohm interferometer.[34] Without a direct hopping between the dots the setup in Fig. 1 E can either be viewed as two dots each having a single level or a single dot with two levels. For certain parameter sets the cases Fig. 1 D and E are equivalent (see below).[32]

The numerical renormalization group (NRG) is a reliable method to investigate physical properties of systems with local Coulomb correlations[35,36] and was very successfully used to study the linear transport through a

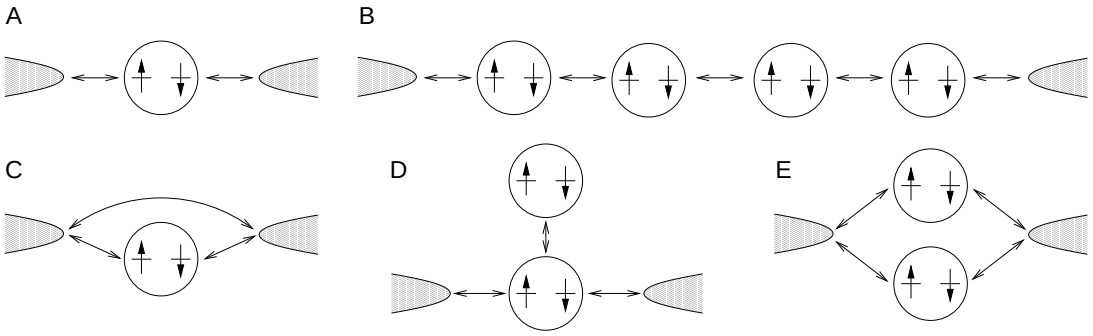

FIG. 1: Dot geometries considered in the present paper.

single-level dot.[20,21,26] Unfortunately, the computational resources required strongly increase with the number of interacting degrees of freedom. This usually limits the applicability of NRG to mesoscopic systems with two spin-degenerate levels[28,29,30,31,32,33] and even in these cases a complete analysis of the parameter dependencies is practically impossible. For a linear chain of dots using special symmetries and a direct relation between the linear conductance and phase shifts it was possible to compute G at $T = 0$ for up to four dots.[22,23]

Thus, alternative reliable methods are needed to systematically investigate parameter dependencies and study more complex systems with a larger number of degrees of freedom. Simple methods such as low-order perturbation theory or the self-consistent Hartree-Fock approximation (SCHFA) already fail to correctly describe the Kondo physics[13] in a single-level dot and are thus inappropriate. Equations-of-motion techniques were successfully used to compute $G(V_g)$ at high temperatures, but even sophisticated decoupling schemes only qualitatively capture the small-T Kondo regime.[37] Similarly, perturbation theory in the coupling of the mesoscopic system to the leads works at large T, but fails for the large conductance resonances at small T.[38] In temperature and parameter regimes in which charge fluctuations dominate a real-time renormalization group method[39] can be used.[31] A zero-temperature method that has frequently been used is exact diagonalization of a small cluster of lattice sites containing the dot followed by an embedding procedure.[40] It has been criticized[28,41] to produce severe artifacts in $G(V_g)$ and even in the case of a single-level dot, where at least the qualitative behavior comes out correctly, the quantitative agreement with NRG data is rather poor.[42] Also the mean-field slave-Boson approach[43] was used, first to study the single-level dot. Within this method $G(V_g)$ falls off too quickly away from the plateau region as compared to the Bethe ansatz and NRG data.[44,45] Furthermore, the method does not capture the correct dependence of $G(V_g)$ on a magnetic field that lifts the spin degeneracy of the single level.[46] Despite these shortcomings the method was also used for more complex dot systems.[47] Recently, a method based on the Gunnarsson-Schönhammer variational approach[48] has been applied to the dot with a spin-degenerate level[49] and a linear chain of three dots.[24] It remains to be seen if this approach can with equal success be used in the presence of a magnetic field and for multi-path systems.

We here propose a novel $T = 0$ approach to study transport through mesoscopic systems with local Coulomb correlations that is based on the functional renormalization group (fRG). The fRG was recently introduced[50] as a new powerful tool for studying interacting Fermi systems. It provides a systematic way of resumming competing instabilities[51] and goes beyond simple perturbation theory even in problems which are not plagued by infrared divergences.[52,53] The fRG procedure we use starts from an exact hierarchy of differential flow equations for the one-particle irreducible vertex functions,[52,54,55,56] i.e., the self-energy, the irreducible 2-particle interaction etc. It is derived by replacing the free propagator by a propagator depending on an infrared cutoff Λ and taking the derivative of the generating functional with respect to Λ. We will apply two different truncation schemes to the models sketched in Fig. 1. Both result in a simple set of coupled differential equations that can easily be integrated numerically and in certain cases even analytically. By an explicit comparison of our results for $G(V_g)$ and the occupancies to NRG and Bethe ansatz data we show that the method works well for surprisingly large U/Γ. The method can easily be extended to other setups and thus provides a useful and reliable tool to investigate transport through quantum dots. In two short publications it was earlier used to compute $G(V_g)$ for a single dot with Luttinger-liquid leads[57] and for a spin-polarized parallel double dot.[33]

This paper is organized as follows. In Sec. II we present our general model. We then derive the fRG flow equations in Sec. III. In Secs. IV-VII we discuss our results for the gate voltage dependence of the linear conductance of the systems of Fig. 1 and for the cases shown in A-D we explicitly compare them to existing NRG and Bethe ansatz data. For each situation we judge the quality of our approximate method and discuss the limits of its applicability. In Secs. V-VII (setup of Fig. 1 B, D, and E) we go beyond situations that have previously been studied and present novel results. We conclude in Sec. VIII with a brief summary and an outlook.

II. THE MODEL

Our general Hamiltonian

$$H = H_{\rm lead} + H_{\rm direct} + H_{\rm dot} + H_{\rm coup} \tag{1}$$

consists of four parts. For simplicity the two leads are assumed to be equal and described by a tight-binding model

$$H_{\rm lead} = -\tau \sum_{\sigma} \sum_{l=L,R} \sum_{m=0}^{\infty} \left(c^{\dagger}_{m,\sigma,l} c_{m+1,\sigma,l} + \text{H.c.} \right) \tag{2}$$

with $c^{(\dagger)}_{m,\sigma,l}$ being the annihilation (creation) operator for an electron with spin direction $\sigma =\uparrow, \downarrow$ localized on lattice site m of the left ($l = L$) or right ($l = R$) lead. The hopping matrix element in the leads is denoted by τ. To describe the system sketched in Fig. 1 C we need a term that directly links the left and right lead

$$H_{\rm direct} = \sum_{\sigma} \left(t_{\rm LR} c^{\dagger}_{0,\sigma,R} c_{0,\sigma,L} + \text{H.c.} \right) . \tag{3}$$

The coupled quantum dots are modeled as

$$\begin{aligned} H_{\rm dot} &= \sum_{\sigma} \sum_{j} \varepsilon_{j,\sigma} d^{\dagger}_{j,\sigma} d_{j,\sigma} \\ &- \sum_{\sigma} \sum_{j>j'} t_{j,j'} d^{\dagger}_{j,\sigma} d_{j',\sigma} + \text{H.c.} \\ &+ \frac{1}{2} \sum_{\sigma,\sigma'} \sum_{j,j'} U^{\sigma,\sigma'}_{j,j'} \left(n_{j,\sigma} - \frac{1}{2} \right) \left(n_{j',\sigma'} - \frac{1}{2} \right) \end{aligned} \tag{4}$$

with annihilation (creation) operators $d^{(\dagger)}_{j,\sigma}$ and the site occupancy $n_{j,\sigma} = d^{\dagger}_{j,\sigma} d_{j,\sigma}$. With this dot Hamiltonian we equally describe multi-level and multi-dot situations or even mixtures of both. The dot or level index j runs from 1 to N. The level positions $\varepsilon_{j,\sigma}$ consist of constant parts $\varepsilon^0_{j,\sigma}$ and a variable gate voltage V_g that is used to shift the energy levels: $\varepsilon_{j,\sigma} = \varepsilon^0_{j,\sigma} + V_g$. Our notation allows for both spin-degenerate levels and levels that are split by a magnetic field. For j's that belong to different dots it is meaningful to introduce nonzero hopping matrix elements $t_{j,j'}$. The 2-particle interaction $U^{\sigma,\sigma'}_{j,j'}$ vanishes for $j = j'$ and $\sigma = \sigma'$. Besides this restriction we allow for both intra-level interactions of spin up and spin down electrons as well as inter-level interactions. Finally, the coupling between dot and lead states is given by

$$H_{\rm coup} = -\sum_{\sigma} \sum_{l=L,R} \sum_{j} (t^l_j c^{\dagger}_{0,\sigma,l} d_{j,\sigma} + \text{H.c.}) \tag{5}$$

with overlaps t^l_j, that enter the energy scale of the dot level broadening $\Gamma^l_j = \pi |t^l_j|^2 \rho_{\rm lead}$, where $\rho_{\rm lead}$ denotes the local density of states at the end of each semi-infinite lead. As usual we later take $\rho_{\rm lead}$ to be energy independent (wide-band limit). The choice of the nonzero t^l_j and $t_{j,j'}$ introduces a spatial geometry between the dots. For ring-like geometries (Fig. 1 C and E) one might also be interested in studying the effect of a magnetic flux piercing the ring. This can be modeled by including appropriate phase factors in the hopping matrix elements $t_{\rm LR}$, t^l_j, $t_{j,j'}$ along the ring.[26,31,33] All the systems shown in Fig. 1 follow from this Hamiltonian by special choices of the parameters. Obviously, it can also be used to model other cases of interest.

III. THE METHOD

Applying the Landauer-Büttiker formalism[59] the $T = 0$ linear conductance for noninteracting electrons can be expressed as

$$G(V_g) = G_{\uparrow}(V_g) + G_{\downarrow}(V_g) , \tag{6}$$

with

$$G_{\sigma}(V_g) = \frac{e^2}{h} \left| \mathcal{T}_{\sigma}(0, V_g) \right|^2 , \tag{7}$$

where the transmission is given by

$$\mathcal{T}_{\sigma}(\varepsilon, V_g) = 2\pi\tau^2 \, \rho_{\rm lead}(\varepsilon) \, \mathcal{G}_{0,\sigma,L;0,\sigma,R}(\varepsilon + i0) \tag{8}$$

and the energy ε is measured relative to the chemical potential μ. Here $\mathcal{G}$ denotes the retarded one-particle Green function (the resolvent in the present single-particle problem) of the system. For the leads described by Eq. (2) the local density of states at site $m = 0$ is (if they are decoupled from the rest of the system)

$$\rho_{\rm lead}(\varepsilon) = \frac{1}{2\pi\,\tau^2} \, \sqrt{4\tau^2 - (\varepsilon + \mu)^2} \; \Theta(2\tau - |\varepsilon + \mu|) . \tag{9}$$

The transmission phase $\alpha_{\sigma}(V_g)$ is given by the phase of $\mathcal{T}_{\sigma}(0, V_g)$.

The noninteracting Green function matrix element involving lead states $\mathcal{G}_{0,\sigma,L;0,\sigma,R}$ can be related to matrix elements involving only the dot states with quantum numbers j, σ and $\rho_{\rm lead}$. The explicit form of this relation depends on the choice of nonzero t^l_j. It can be obtained using a standard projection technique[60] and is based on the relation

$$\begin{aligned} &P \mathcal{G}_{1p}(z) P \; = \\ &\left[zP - PH_{1p}P - PH_{1p}Q \left(zQ - QH_{1p}Q \right)^{-1} QH_{1p}P \right]^{-1} , \end{aligned} \tag{10}$$

where H_{1p} is an arbitrary single-particle Hamiltonian, $\mathcal{G}_{1p}(z) = [z - H_{1p}]^{-1}$ the resolvent, and P, Q are projectors with $P + Q = \mathbf{1}$.

For Fermi liquids, as discussed here, the same $T = 0$ relations Eqs. (6)-(8) between matrix elements of the one-particle Green function and the conductance hold in the presence of interactions.[61] To obtain G_{σ} and α_{σ} we thus have to determine the one-particle Green function of the

dot system in the presence of the interaction and the leads. From this also the level occupancies $\langle n_{j,\sigma}\rangle$ can be determined by integrating $\mathcal{G}_{j,\sigma;j,\sigma}(z)$ along the imaginary axis.[62]

As a first step we integrate out the noninteracting leads within a functional integral representation of our many-body problem.[62] They provide a frequency dependent one-particle potential for those indices j for which $t^l_j \neq 0$. On the imaginary frequency axis it is given by

$$V^{\rm lead}_{j,\sigma;j',\sigma'}(i\omega) = \sum_l t^l_j \left(t^l_{j'}\right)^* {\rm g}_{\rm lead}(i\omega)\, \delta_{\sigma,\sigma'} \;, \qquad (11)$$

where ${\rm g}_{\rm lead}(i\omega)$ denotes the spin-independent Green function of the isolated semi-infinite leads taken at the last lattice site

$${\rm g}_{\rm lead}(i\omega) = \frac{i\omega+\mu}{2\,\tau^2}\left(1-\sqrt{1-\frac{4\,\tau^2}{(i\omega+\mu)^2}}\right) \;. \qquad (12)$$

After this step, instead of dealing with an infinite system we only have to consider the dot system of N interacting levels. We here take $\mu = 0$. In the computation of the Green function projected onto the dot system the sum of the dot Hamiltonian at $U^{\sigma,\sigma'}_{j,j'} = 0$ and $V^{\rm lead}_{j,j'}(i\omega)$ can be interpreted as a frequency dependent "effective Hamiltonian" and in the following will be denoted by $h(i\omega)$.

We now set up our fRG scheme. As a first step we replace the noninteracting dot propagator $\mathcal{G}_0$, as obtained from Eq. (4) and the projection of the leads, by a cutoff-dependent propagator that suppresses the infrared modes with Matsubara frequency $|\omega| < \Lambda$,

$$\mathcal{G}^\Lambda_0(i\omega) = \Theta(|\omega|-\Lambda)\mathcal{G}_0(i\omega) = \Theta(|\omega|-\Lambda)\left[i\omega - h(i\omega)\right]^{-1} \qquad (13)$$

with Λ running from ∞ down to 0. For convenience we use a sharp cutoff (see below). Using $\mathcal{G}^\Lambda_0$ in the generating functional of the irreducible vertex functions[62] and taking the derivative with respect to Λ one can derive an exact, infinite hierarchy of coupled differential equations for vertex functions, such as the self-energy and the irreducible 2-particle interaction. In particular, the flow of the self-energy Σ^Λ (1-particle vertex) is determined by Σ^Λ and the 2-particle vertex Γ^Λ, while the flow of Γ^Λ is determined by Σ^Λ, Γ^Λ, and the flowing 3-particle vertex Γ^Λ_3. The latter could be computed from a flow equation involving the 4-particle vertex, and so on. At the end of the fRG flow $\Sigma^{\Lambda=0}$ is the self-energy Σ of the original, cutoff-free problem we are interested in.[52,56,65] A detailed derivation of the fRG flow equations for a general quantum many-body problem that only requires a basic knowledge of the functional integral approach to many-particle physics[62] and the application of the method for a simple toy problem are presented in Ref. 63. In practical applications the hierarchy of flow equations has to be truncated and $\Sigma^{\Lambda=0}$ only provides an approximation for the exact Σ. As a first approximation we here neglect the 3-particle vertex (irreducible 3-particle interaction). The contribution of Γ^Λ_3 to Γ^Λ is small as long as Γ^Λ is small, because Γ^Λ_3 is initially (at $\Lambda = \infty$) zero and is generated only from terms of third order in Γ^Λ. Furthermore, Γ^Λ stays small for all Λ if its initial values $U^{\sigma,\sigma'}_{j,j'}$ (for the details of the initial conditions, see below) are not too large. By explicit comparison to NRG data below we will clarify the meaning of "not-too-large" in the cases of interest. This approximation leads to a closed set of equations for Γ^Λ and Σ^Λ given by

$$\frac{\partial}{\partial\Lambda}\Sigma^\Lambda(1',1) = -\frac{1}{2\pi}\sum_{2,2'} e^{i\omega_2 0^+}\, S^\Lambda(2,2')\,\Gamma^\Lambda(1',2';1,2) \qquad (14)$$

and

$$\begin{aligned}\frac{\partial}{\partial\Lambda}\Gamma^\Lambda(1',2';1,2) = {}& \frac{1}{2\pi}\sum_{3,3'}\sum_{4,4'}\mathcal{G}^\Lambda(3,3')\,S^\Lambda(4,4') \\ &\times\Big[\Gamma^\Lambda(1',2';3,4)\,\Gamma^\Lambda(3',4';1,2) \\ &-\Gamma^\Lambda(1',4';1,3)\,\Gamma^\Lambda(3',2';4,2) - (3\leftrightarrow 4, 3'\leftrightarrow 4') \\ &+\Gamma^\Lambda(2',4';1,3)\,\Gamma^\Lambda(3',1';4,2) + (3\leftrightarrow 4, 3'\leftrightarrow 4')\Big] \;. \end{aligned} \qquad (15)$$

The labels 1, 2, etc., are a shorthand for the quantum numbers of the one-particle basis j,σ and the Matsubara frequencies and the summation stands for a sum over the quantum numbers and an integral over the frequency. The full propagator $\mathcal{G}^\Lambda$ is given by the Dyson equation

$$\mathcal{G}^\Lambda = \left[(\mathcal{G}^\Lambda_0)^{-1} - \Sigma^\Lambda\right]^{-1} \qquad (16)$$

and the so-called single-scale propagator S^Λ by

$$S^\Lambda = \mathcal{G}^\Lambda\left[\frac{\partial}{\partial\Lambda}\left(\mathcal{G}^\Lambda_0\right)^{-1}\right]\mathcal{G}^\Lambda \;. \qquad (17)$$

The order of the projection onto the system of dots and the introduction of a cutoff can equally be interchanged, leading to the same set of flow equations.

We next implement our second approximation: the frequency-dependent flow of the renormalized 2-particle vertex Γ^Λ is replaced by its value at vanishing (external) frequencies, such that Γ^Λ remains frequency independent. Since the bare interaction is frequency independent, neglecting the frequency dependence leads to errors only at second order (in the interaction strength) for the self-energy, and at third order for the vertex function at zero frequency. As a consequence, also the self-energy becomes frequency independent. Then $\varepsilon_{j,\sigma} + \Sigma_{j,\sigma;j,\sigma}$ can be viewed as the effective (single-particle) level position and $t_{j,j'} + \Sigma_{j,\sigma;j',\sigma}$, with $j \neq j'$ as the effective (single-particle) hopping between the levels. In general both depend on all parameters of the problem, in particular the two-particle interaction. This interpretation will later be helpful to gain further insights in our results.

For a sharp frequency cutoff the frequency integrals on the right-hand side (rhs) of the flow equations (14) and (15) can be carried out analytically. At this point one has to deal with products of delta functions $\delta(|\omega|-\Lambda)$ and

expressions involving step functions $\Theta(|\omega|-\Lambda)$. These at first sight ambiguous expressions are well defined and unique if the sharp cutoff is implemented as a limit of increasingly sharp broadened cutoff functions Θ_ϵ, with the broadening parameter ϵ tending to zero. The expressions can then be conveniently evaluated by using the following relation,[55] valid for arbitrary continuous functions f:

$$\delta_\epsilon(x-\Lambda)\, f[\Theta_\epsilon(x-\Lambda)] \to \delta(x-\Lambda)\int_0^1 f(t)\, dt\ , \quad (18)$$

where $\delta_\epsilon = \Theta_\epsilon'$. Note that the functional form of Θ_ϵ for finite ϵ does not affect the result in the limit $\epsilon \to 0$. For the approximate flow equations we then obtain

$$\frac{\partial}{\partial\Lambda}\Sigma^\Lambda_{1',1} = -\frac{1}{2\pi}\sum_{\omega=\pm\Lambda}\sum_{2,2'} e^{i\omega 0^+}\,\tilde{\mathcal{G}}^\Lambda_{2,2'}(i\omega)\,\Gamma^\Lambda_{1',2';1,2} \quad (19)$$

and

$$\frac{\partial}{\partial\Lambda}\Gamma^\Lambda_{1',2';1,2} = \frac{1}{2\pi}\sum_{\omega=\pm\Lambda}\sum_{3,3'}\sum_{4,4'}\Big\{\frac{1}{2}\,\tilde{\mathcal{G}}^\Lambda_{3,3'}(i\omega)\,\tilde{\mathcal{G}}^\Lambda_{4,4'}(-i\omega)\;\Gamma^\Lambda_{1',2';3,4}\,\Gamma^\Lambda_{3',4';1,2} + \tilde{\mathcal{G}}^\Lambda_{3,3'}(i\omega)\,\tilde{\mathcal{G}}^\Lambda_{4,4'}(i\omega) \times\Big[-\Gamma^\Lambda_{1',4';1,3}\,\Gamma^\Lambda_{3',2';4,2} + \Gamma^\Lambda_{2',4';1,3}\,\Gamma^\Lambda_{3',1';4,2}\Big]\Big\} \quad (20)$$

where the lower indexes 1, 2, etc. now stand for the single-particle quantum numbers j,σ (not frequencies) and

$$\tilde{\mathcal{G}}^\Lambda(i\omega) = \big[\mathcal{G}_0^{-1}(i\omega) - \Sigma^\Lambda\big]^{-1}\ . \quad (21)$$

Note that in contrast to $\mathcal{G}^\Lambda$ in Eq. (16), $\tilde{\mathcal{G}}^\Lambda$ contains the cutoff-free noninteracting propagator. Thus, by taking a sharp cutoff the explicit cutoff function completely disappears from the flow equation, making it smooth and easy to integrate numerically.[65] At the initial cutoff $\Lambda=\infty$ the flowing 2-particle vertex $\Gamma^\Lambda_{1',2';1,2}$ is given by the antisymmetrized interaction (see below). Equation (15) preserves the antisymmetry under the exchange of the first and second two indices. This reduces the number of independent $\Gamma^\Lambda_{1',2';1,2}$. Furthermore, Eq. (20) preserves the spin conservation of the Hamiltonian. One can either use these symmetries to reduce the number of both, flow equations and independent summations on the rhs of Eq. (20), or directly implement this equation for simplicity. In complex cases the first will considerably speed up the numerical integration of the flow equations. To exemplify this we consider the single-level case. Then the only physical interaction is the one between spin up and spin down electrons and Eq. (20) reduces to a single equation with no sum over quantum numbers left on the rhs.

The flow is determined uniquely by the differential flow equations and the initial conditions at $\Lambda=\infty$. The flow of the 2-particle vertex starts from the antisymmetrized bare 2-particle interaction[62] $I_{1',2';1,2}$ while m-particle vertices of higher order vanish in the absence of bare m-body interactions with $m>2$. The self-energy at $\Lambda=\infty$ is given by the bare one-particle potential, that is, by those one-particle terms which are not included already in $\mathcal{G}_0$. For fixed quantum numbers j,σ in Eq. (4) these are terms of the form $-\sum_{\sigma',j'} U^{\sigma,\sigma'}_{j,j'}/4$. In a numerical solution the flow starts at some large finite initial cutoff Λ_0. Here one has to take into account that, due to the slow decay of the rhs of the flow equation for Σ^Λ at large Λ, the integration of the flow from $\Lambda=\infty$ to $\Lambda=\Lambda_0$ yields a contribution which does not vanish in the limit $\Lambda_0\to\infty$, but rather tends to a finite constant. Since $\tilde{\mathcal{G}}^\Lambda_{2,2'}(i\omega)\to\delta_{2,2'}/(i\omega)$ for $|\omega|=\Lambda\to\infty$, this constant is easily determined as

$$-\frac{1}{2\pi}\lim_{\Lambda_0\to\infty}\int_\infty^{\Lambda_0} d\Lambda\sum_{\omega=\pm\Lambda}\sum_{2,2'} e^{i\omega 0^+}\,\frac{\delta_{2,2'}}{i\omega}\,I_{1',2';1,2} = \frac{1}{2}\sum_2 I_{1',2;1,2}\ . \quad (22)$$

This exactly cancels the bare one-particle term (see above). In summary, the initial conditions for the self-energy and the 2-particle vertex at $\Lambda=\Lambda_0\to\infty$ are

$$\Sigma^{\Lambda_0}_{1,1'} \;=\; 0 \quad (23)$$

$$\Gamma^{\Lambda_0}_{1',2';1,2} \;=\; I_{1',2';1,2}\ . \quad (24)$$

For the flow at $\Lambda<\Lambda_0$ the factor $e^{i\omega 0^+}$ in Eq. (19) can be discarded.

In the following sections we use the above fRG-based approximation scheme to study the conductance, the transmission phase, and the level occupancies for the geometries sketched in Fig. 1. For the single-dot case we also apply an even simpler scheme for comparison, where the flowing 2-particle vertex is replaced by its initial value. The system of flow equations then reduces to Eq. (19).

IV. SINGLE DOTS

As a first example we study the single dot case of Fig. 1 A. Since $N=1$ we suppress the dot index $j=1$. Fur-

thermore, the Hamiltonian conserves the spin and the self-energy and Green function is diagonal in the spin index σ. The same holds for the other setups studied. The level energies are $\varepsilon_\uparrow = V_g - \mathcal{H}/2$, $\varepsilon_\downarrow = V_g + \mathcal{H}/2$, where $\mathcal{H}$ denotes a magnetic field, and the interaction between up and down electrons occupying the dot level is U. We here consider the case with left-right symmetry of the level-lead hoppings $t^L = t^R = t'$, but the results can easily be generalized. Note that due to the shift of the density by $-1/2$ in the last line of Eq. (4), $V_g = 0$ corresponds to half filling of the dot. The projected noninteracting propagator is given by[13]

$$\mathcal{G}_{0,\sigma}(i\omega) = \frac{1}{i\omega - (V_g + \sigma\mathcal{H}/2) + i\Gamma\,\mathrm{sgn}(\omega)}\,, \qquad (25)$$

where on the rhs $\sigma = \uparrow = +1$ and $\sigma = \downarrow = -1$. We have performed the wide-band limit that leads to an energy-independent hybridization $\Gamma = \Gamma^L + \Gamma^R = 2\pi t'^2 \rho_{\rm lead}$. This is achieved by replacing $\tau \to \eta\tau$ and $t' \to \sqrt{\eta}t'$ and taking $\eta \to \infty$. The flow equations for the effective level positions $V_\sigma^\Lambda = V_g + \sigma\mathcal{H}/2 + \Sigma_\sigma^\Lambda$ are

$$\begin{aligned}\frac{\partial}{\partial\Lambda}V_\sigma^\Lambda &= -\frac{U^\Lambda}{2\pi}\sum_{\omega=\pm\Lambda}\tilde{\mathcal{G}}_{\bar\sigma}^\Lambda(i\omega) \\ &= \frac{U^\Lambda\, V_{\bar\sigma}^\Lambda/\pi}{(\Lambda+\Gamma)^2 + (V_{\bar\sigma}^\Lambda)^2}\,, \end{aligned} \qquad (26)$$

with the initial condition $V_\sigma^{\Lambda=\infty} = V_g + \sigma\mathcal{H}/2$ and $\bar\sigma$ denoting the complement of σ. The cutoff-dependent propagator $\tilde{\mathcal{G}}_\sigma^\Lambda(i\omega)$ follows from $\mathcal{G}_{0,\sigma}(i\omega)$ by replacing $V_g + \sigma\mathcal{H}/2 \to V_\sigma^\Lambda$. As already mentioned above, using symmetries the flow of the 2-particle vertex can be reduced to a single equation for the effective interaction between spin up and spin down electrons U^Λ. It is defined by $U^\Lambda = \Gamma^\Lambda_{\sigma,\bar\sigma;\sigma,\bar\sigma}$, has the flow equation

$$\begin{aligned}\frac{\partial}{\partial\Lambda}U^\Lambda &= \frac{(U^\Lambda)^2}{2\pi}\sum_{\omega=\pm\Lambda}\left[\tilde{\mathcal{G}}_\uparrow^\Lambda(i\omega)\,\tilde{\mathcal{G}}_\downarrow^\Lambda(-i\omega) + \tilde{\mathcal{G}}_\uparrow^\Lambda(i\omega)\,\tilde{\mathcal{G}}_\downarrow^\Lambda(i\omega)\right] \\ &= \frac{2\,\left(U^\Lambda\right)^2\, V_\uparrow^\Lambda\, V_\downarrow^\Lambda/\pi}{\left[(\Lambda+\Gamma)^2 + (V_\uparrow^\Lambda)^2\right]\left[(\Lambda+\Gamma)^2 + (V_\downarrow^\Lambda)^2\right]}\,, \end{aligned} \qquad (27)$$

and initial condition $U^{\Lambda=\infty} = U$.

Within this approximation the dot spectral function at the end of the fRG flow is given by

$$\rho_\sigma(\omega) = \frac{1}{\pi}\,\frac{\Gamma}{\left(\omega - V_\sigma\right)^2 + \Gamma^2}\,, \qquad (28)$$

with $V_\sigma = V_\sigma^{\Lambda=0}$, that is a Lorentzian of full width 2Γ and height $1/(\pi\Gamma)$ centered around V_σ. For the single dot, instead of using Eq. (8) the transmission can be expressed in terms of the dot spectral weight at the chemical potential[64]

$$G_\sigma(V_g) = \frac{e^2}{h}\,\pi\Gamma\,\rho_\sigma(0)\,. \qquad (29)$$

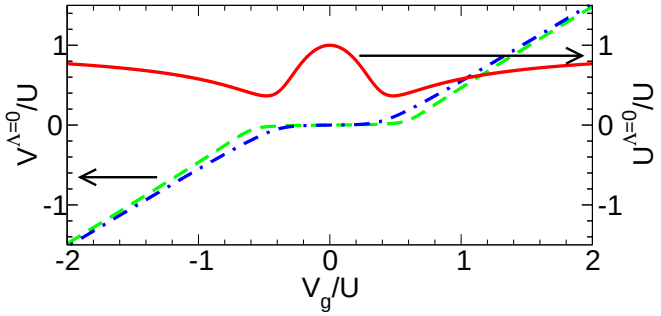

FIG. 2: (Color online) Gate Voltage dependence of the effective level position and interaction for a single-level dot at $U/\Gamma = 4\pi$ and $\mathcal{H} = 0$. Dashed line: $V = V^{\Lambda=0}$ without flow of the interaction. Dashed-dotted line: $V = V^{\Lambda=0}$ with flow of the interaction. Solid line: effective interaction $U^{\Lambda=0}$.

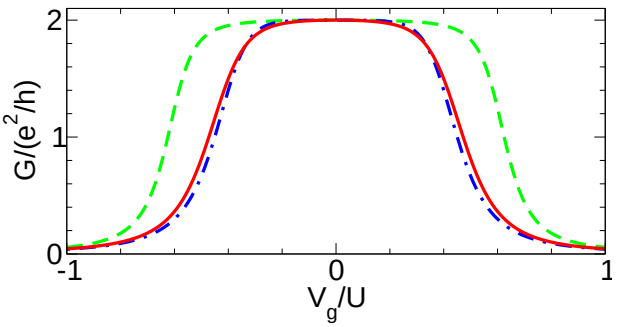

FIG. 3: (Color online) Gate Voltage dependence of the linear conductance for the same parameters as in Fig. 2. Solid line: exact Bethe ansatz solution from Ref. 21. Dashed line: fRG approximation without flow of the interaction. Dashed-dotted line: fRG approximation with flow of vertex.

Within our approximation the spectral weight and thus the conductance directly follows from the effective level position V_σ at the end of the fRG flow.

In the following we consider strong couplings $U/\Gamma \gg 1$ and start out with the case $\mathcal{H} = 0$. The latter implies that $V_\uparrow^\Lambda = V_\downarrow^\Lambda = V^\Lambda$ and $G_\uparrow = G_\downarrow$. The spectral function computed at $V_g = 0$ using NRG (that is believed to be very close to the exact spectral function) shows a sharp Kondo resonance of height $1/(\pi\Gamma)$ and width T_K, where T_K is the Kondo temperature, located around $\omega = 0$. It has two additional broader features at $\omega = \pm U/2$ (Hubbard bands). For $-U/2 \lessapprox V_g \lessapprox U/2$ the Kondo peak is pinned at (close to) the chemical potential and has fixed height.[13] Using Eq. (29) this leads to the plateau of width U in $G(V_g)$ discussed in the introduction. Although our approximate spectral function neither shows the narrow Kondo resonance nor the Hubbard bands, we show that by a pinning of V_σ it captures the pinning of the spectral weight. We reproduce the line shape of the conductance quantitatively up to very large U/Γ.

To gain some analytical insight we first replace $U^\Lambda \to U$ and solve Eq. (26). The solution is obtained in implicit

form

$$\frac{vJ_1(v)-\gamma J_0(v)}{vY_1(v)-\gamma Y_0(v)}=\frac{J_0(v_g)}{Y_0(v_g)}\,, \tag{30}$$

with $v=V\pi/U$, $v_g=V_g\pi/U$, $\gamma=\Gamma\pi/U$, and Bessel functions J_n, Y_n. For $|V_g|<V_c$, with $v_c=V_c\pi/U$ being the first zero of J_0, i.e., $V_c=0.7655\,U$, this equation has a solution with a small $|V|$. For $U\gg\Gamma$ the crossover to a solution with $|V|$ being of order U (for $|V_g|>V_c$) is fairly sharp. Expanding both sides of Eq. (30) for small $|v|$ and $|v_g|$ gives $V=V_g\exp[-U/(\pi\Gamma)]$. Inserting this in Eq. (28) leads to an exponential pinning of the spectral weight at μ. In Fig. 2 we show $V(V_g)$ for $U/\Gamma=4\pi$ as the dashed line. For $|V_g|\gg U/2$ we find $V=V_g-\mathrm{sgn}(V_g)\,U/2$. Applying Eq. (29) the exponential pinning of the spectral weight at $\mu=0$ for small $|V_g|$ and the sharp crossover to a V of order U when $|V_g|>V_c$ leads to the plateau in $G(V_g)$ shown as the dashed line in Fig. 3. For $U\gg\Gamma$ the width of the plateau is $2V_c=1.531U$, which is larger than the width U found from the exact Bethe ansatz solution[21] (solid line in Fig. 3) and with NRG.

This can systematically be improved including the flow of the interaction Eq. (27). As the dashed-dotted and solid lines in Fig. 2 we show the effective level position and the effective interaction at the end of the fRG flow. The dashed-dotted line in Fig. 3 is the resulting $G(V_g)$. Away from $V_g=0$ the effective interaction first decreases and the plateau becomes narrower. The approximate conductance then agrees quantitatively with the exact Bethe ansatz result (solid line in Fig. 3). For decreasing U/Γ the agreement of fRG and Bethe ansatz data systematically improves and for $U/\Gamma\lessapprox 6$ the two curves can barely be distinguished. The agreement becomes only slightly worse than in Fig. 3 for U/Γ as large as 25, the largest U/Γ for which Bethe ansatz data are available in the literature.[21] Also for more complex dot geometries including the flow of the effective interaction considerably improves the agreement with NRG and from now on we exclusively use this truncation scheme.

We next consider the case of finite magnetic fields. For $\mathcal{H}>0$ the Kondo resonance in the NRG solution of the spectral function splits in two peaks with a dip at $\omega=0$, resulting in a dip of $G(V_g)$ at $V_g=0$. In Figs. 4 and 5 we compare the total $G=G_\uparrow+G_\downarrow$ and partial $G_\uparrow$ conductance obtained from our fRG truncation scheme including the flow of the interaction and from NRG[66] for $U/\Gamma=3\pi$ and different $\mathcal{H}$. In the caption we give $\mathcal{H}$ in units of $T_K^{NRG}=0.116\Gamma$, where T_K^{NRG} is determined from the width of the Kondo resonance at the particle-hole symmetric point $V_g=0$ using NRG.[66] The agreement between NRG and fRG results is excellent. In particular, at $V_g=0$ the NRG and fRG data for $\mathcal{H}=T_K^{NRG}$ are almost indistinguishable.

This observation suggest that our approximate scheme indeed contains the Kondo temperature T_K that depends exponentially on a combination of U and the level

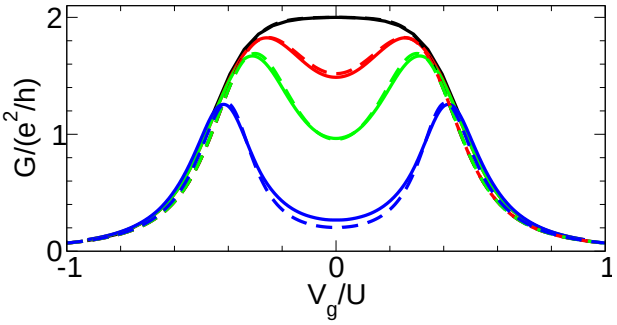

FIG. 4: (Color online) Gate Voltage dependence of the total conductance G of a single dot with $U/\Gamma=3\pi$ and $\mathcal{H}/\Gamma=0$, 0.058, 0.116, 0.58 from top to bottom. In units of the $V_g=0$ Kondo temperature $T_K^{NRG}/\Gamma=0.116$ these fields correspond to $\mathcal{H}=0$, $0.5T_K^{NRG}$, T_K^{NRG}, and $5T_K^{NRG}$. Solid line: NRG data from Ref. 66. Dashed line: fRG approximation with flow of vertex.

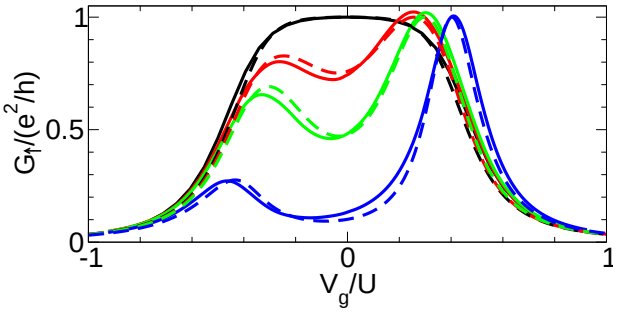

FIG. 5: (Color online) Gate Voltage dependence of the partial conductance $G_\uparrow$ of a single dot for the same parameters as in Fig. 4.

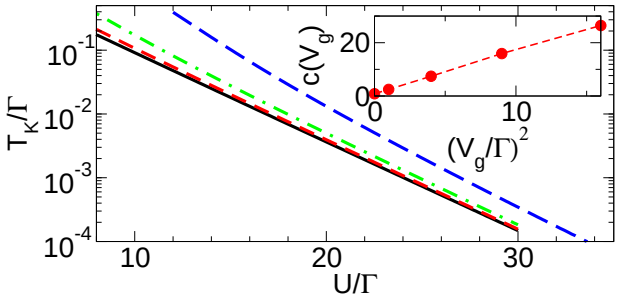

FIG. 6: (Color online) The Kondo scale T_K as a function of U for different V_g: $V_g=0$ (solid), $V_g/\Gamma=1$ (short dashed), $V_g/\Gamma=2$ (dashed-dotted), and $V_g/\Gamma=4$ (long dashed). *Inset:* The fitting parameter c as a function of $(V_g/\Gamma)^2$.

position[13]

$$\begin{aligned} T_K^{exact} &\sim \exp\left[-\frac{\pi}{2U\Gamma}\left|U^2/4-V_g^2\right|\right] \\ &= \exp\left[-\left|\frac{\pi}{8}\frac{U}{\Gamma}-\frac{\pi}{2}\frac{V_g^2}{\Gamma^2}\frac{\Gamma}{U}\right|\right]. \end{aligned} \tag{31}$$

The prefactor of the exponential depends on the details of the model considered. To leading order its U and V_g dependence can be neglected. To investigate the appearance of an exponentially small energy scale within our

approximation we define a Kondo scale $T_K(U, V_g)$ by the magnetic field required to suppress the total conductance down to half the unitary limit $G(U, V_g, \mathcal{H} = T_K) = e^2/h$. For fixed $U \gg \Gamma$ this definition is meaningful for gate voltages which for $\mathcal{H} = 0$ are in the conductance plateau. In Fig. 6 we show $T_K(U, V_g)$ for different V_g as a function of U on a linear-log scale. The curves can be fitted by a function of the form [see Eq. (31)]

$$f(U/\Gamma) = a \exp\left[-\left|b\frac{U}{\Gamma} - c\frac{\Gamma}{U}\right|\right]$$

with V_g dependent coefficients a, b, and c. On the scale of Fig. 6 the original data and the fits are indistinguishable. We find that $b(V_g)$ barely changes with V_g and is given by $b \approx 0.32$, which is close to the exact value $\pi/8 \approx 0.39$ [see Eq. (31)]. Furthermore, the prefactor a depends only weakly on V_g and $c(V_g)$ increases approximately quadratically with V_g/Γ as shown in the inset of Fig. 6. Both these results are consistent with the behavior of the exact Kondo temperature Eq. (31). We thus conclude that $T_K(U, V_g)$ can be estimated from the $\mathcal{H}$ dependence of G obtained within the fRG. The Kondo temperature can also be obtained from the local spin susceptibility.[13] Computing this using our fRG scheme leads to results equivalent to the ones discussed above.

For the single dot at $T = 0$ the exact conductance, transmission phase, and dot occupancies are directly related by a generalized Friedel sum rule:[13] $G_\sigma/(e^2/h) = \sin^2(\pi \langle n_\sigma \rangle)$, $\alpha_\sigma = \pi \langle n_\sigma \rangle$. As $0 \leq \langle n_\sigma \rangle \leq 1$ the argument of $\sin^2$ is restricted to a single period and the relation between G_σ, $\langle n_\sigma \rangle$, and α_σ is unique. In many approximation schemes the Friedel sum rule does not hold exactly. Within our method we map the many-body problem onto an effective single-particle one for which the Friedel sum rule is fulfilled. For gate voltages within the $\mathcal{H} = 0$ conductance plateau the (spin independent) dot filling is 1/2 and the (spin independent) phase is $\pi/2$. For sufficiently large U/Γ the crossover to $\langle n_\sigma \rangle = 1$ and $\alpha_\sigma = \pi$ to the left of the plateau as well as $\langle n_\sigma \rangle = 0$ and $\alpha_\sigma = 0$ to the right is fairly sharp.

As a more complex single-dot problem we study the case of a dot embedded between two leads, that are also coupled directly (see Fig. 1 C). In that case the conductance shows the characteristics of both the Kondo and the Fano effect, as was discussed earlier based on NRG results.[26] We here focus on $\mathcal{H} = 0$.

To derive expressions for the dot Green function and the conductance we first consider a three-site system of the dot and the last sites of the left and right leads. The effect of the other lead sites is taken into account by projecting them out, which leads to a single-particle potential on the last sites of the leads similar to Eq. (11) but with t_j^l replaced by τ. At $U = 0$ the projected "effective Hamiltonian" [see Eq. (10)] for both spin directions reads (for the hopping between the leads and dot we still assume $t^L = t^R = t'$)

$$h_\sigma(i\omega) = \begin{pmatrix} \tau^2 \mathrm{g}_{\mathrm{lead}}(i\omega) & t_{LR} & -t' \\ t_{LR} & \tau^2 \mathrm{g}_{\mathrm{lead}}(i\omega) & -t' \\ -t' & -t' & V_g \end{pmatrix} \qquad (32)$$

in a basis left lead—right lead—dot. We here consider $t', t_{LR} \in \mathbb{R}$ (for the model with an enclosed magnetic flux, see below). The Green function matrix element entering Eq. (8) is given by the $1-2$ matrix element of the resolvent of $h_\sigma(i\omega)$, Eq. (32). Within our truncation scheme the same holds for $U > 0$ if V_g is replaced by the effective dot level position $V^{\Lambda=0}$ in $h_{3,3}(i\omega)$. To determine the flow equations for V^Λ and U^Λ we employ Eq. (10) a second time and project onto the dot site. After taking the wide-band limit the cutoff-dependent dot Green function is

$$\tilde{\mathcal{G}}_\sigma^\Lambda(i\omega) = \left[i\omega - V^\Lambda + \Gamma \frac{\tilde{t}_{LR} + i\,\mathrm{sgn}(\omega)}{1 + \tilde{t}_{LR}^2}\right]^{-1}, \qquad (33)$$

with $\tilde{t}_{LR} = \pi t_{LR} \rho_{\mathrm{lead}}$. The first lines of Eqs. (26) and (27) also hold in the presence of the direct hopping t_{LR}, which completes the derivation of the flow equations.

At $U = 0$ the interference of the direct energy independent transmission channel and the resonant channel leads to a Fano line shape of $G(V_g)$.[25] The line shape resulting from the presence of both the Kondo and the Fano effect is shown in Fig. 7 for[26] $U/\Gamma \approx 5.05\pi$ and different strength of the direct hopping between the left and right lead. The latter is measured by the $U = 0$ transmission probability $\mathcal{T}_{LR}(t_{LR})$ that would result if only the direct link would be present, that is for $t' = 0$. For $\mathcal{T}_{LR} = 0$ one recovers the single-dot problem discussed above. In the opposite limit of perfect direct transmission $\mathcal{T}_{LR} = 1$ the $U = 0$ Fano anti-resonance at $V_g = 0$ (see the $q = 0$ curve in Fig. 1 of Ref. 25) is extended to a broad region with $G(V_g) \approx 0$ due to the presence of the Kondo effect. The results for $0 < \mathcal{T}_{LR} < 1$ lie in between these two limiting cases. The fRG data again agree well with the NRG results.

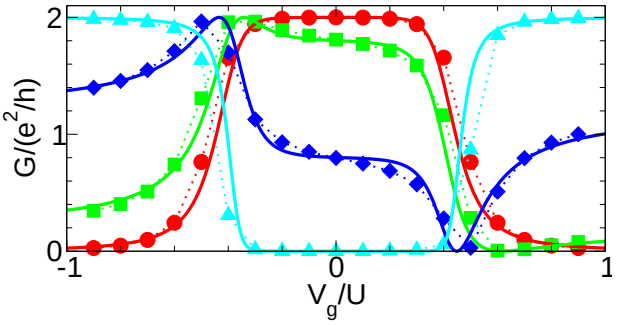

FIG. 7: (Color online) Gate Voltage dependence of the total conductance G of a single dot in the Fano geometry of Fig. 1 C with $U/\Gamma \approx 5.05\pi$, $\mathcal{H} = 0$, and different $\mathcal{T}_{LR}$. Symbols: NRG data from Ref. 26 (circles $\mathcal{T}_{LR} = 0$, squares $\mathcal{T}_{LR} = 0.1$, diamonds $\mathcal{T}_{LR} = 0.6$, triangles $\mathcal{T}_{LR} = 1$). Solid lines: fRG approximation with flow of vertex.

Similar to the single dot without a direct link for the present geometry one can derive unique relations between the conductance, the transmission phase, and the occupancy.[26] Thus the last two observables do not carry any additional information and we do not show them here. In addition to the gate voltage dependence also the dependence on an enclosed magnetic flux was studied. Replacing $t_{LR} \to \exp(i\phi)\, t_{LR}$ a flux can easily be included in our approach and we reproduce the results of Ref. 26.

Our results for the single-level dot show that although the fRG truncation scheme is set up for small U, it works quantitatively for very large U. For $\mathcal{H} = 0$ the method captures the aspect of Kondo physics essential to obtain the plateau in $G(V_g)$, namely the pinning of spectral weight. From this one can expect that the method gives reliable results also for more complex dot systems, as will be explored below. Using a truncation scheme in which the full frequency dependence of the 2-particle vertex is kept (leading to a frequency dependent self-energy) it was shown that one can also reproduce the Kondo resonance and Hubbard bands of the spectral function,[52] although with a much higher numerical effort.[67]

V. LINEAR CHAINS OF DOTS

We next study a linear chain of N single-level dots as shown in Fig. 1 B. For this problem one already has to specify a variety of parameters. The inter-dot hopping matrix elements might not only be restricted to nearest neighbors but extend over a longer range. Depending on the experimental realization of the chain in addition the hoppings of equal range might not all be the same but explicitly depend on the pair of dots considered. Besides the on-site interaction (that might depend on j) one could introduce longer-range interactions. The on-site energies $\varepsilon_{j,\sigma}$ might vary from site to site. Within our approach all these situations can be investigated, as the parameters only enter the projected noninteracting propagator and the initial conditions for the 2-particle vertex. We here consider the cases $N = 3$ and $N = 4$, but also $N = 10$ has been studied with our method. We focus on $\mathcal{H} = 0$, nearest-neighbor inter-dot hoppings of equal amplitude, equal on-site energies, and equal local interactions. We verified that including a nearest-neighbor interaction and a small variation of the inter-dot hoppings only weakly affects our results.

At $U = 0$ the projected "effective Hamiltonian" is a tridiagonal $N \times N$ matrix with off-diagonal entries

$$h_{\sigma;j,j\pm1}(i\omega) = -t \tag{34}$$

and diagonal elements

$$h_{\sigma;j,j}(i\omega) = V_g - i\,\mathrm{sgn}(\omega)\left(\Gamma_1^L\delta_{j,1} + \Gamma_N^R\delta_{j,N}\right) . \tag{35}$$

The (spin-independent) projected noninteracting propagator then follows from the matrix inversion

$$\mathcal{G}_{0,\sigma}(i\omega) = \left[i\omega - h_\sigma(i\omega)\right]^{-1} . \tag{36}$$

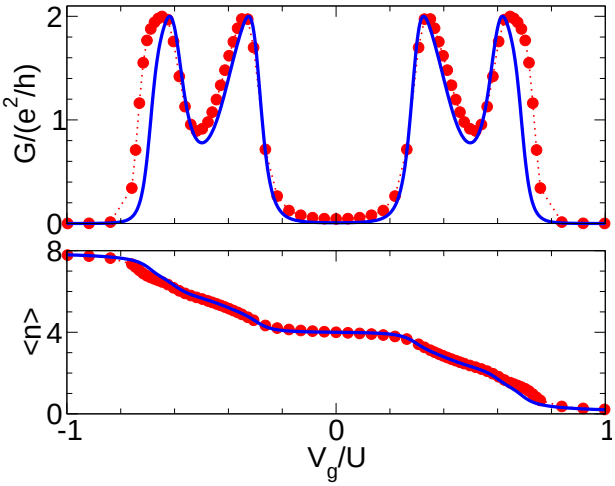

FIG. 8: (Color online) Gate Voltage dependence of the conductance G and the total occupancy $\langle n\rangle$ of a linear chain of $N = 4$ spin-degenerate dots (see Fig. 1 B) with $U/\Gamma = 2\pi$ and $t/\Gamma = 1$. Circles: NRG data from Ref. 23. Solid line: fRG approximation with flow of vertex.

The flow equations for the present setup are obtained by inserting this $\mathcal{G}_0$ into Eq. (21) and using the resulting cutoff-dependent full propagator in Eqs. (19) and (20). The initial conditions are given by Eqs. (23) and (24). Although we start out with a purely local interaction, during the fRG flow Eq. (20) all types of two-particle interactions not forbidden by spin conservation and antisymmetry of the vertex, e.g., long-range density-density interactions and pair hoppings, are generated in $\Gamma^\Lambda_{j_1',\sigma_1',j_2',\sigma_2';j_1,\sigma_1,j_2,\sigma_2}$. We observe the same for the setups of Figs. 1 D and E. With this 2-particle vertex the flowing self-energy Eq. (19) becomes a full $N\times N$ matrix. During the fRG flow the interaction does not only lead to a renormalization of the level positions and the nearest-neighbor hoppings, but also generates longer-range single-particle hoppings. Applying Eqs. (6)-(10) the conductance can be computed from the $1-N$ matrix element of the projected Green function at $\Lambda = 0$ by (note that $\tilde{\mathcal{G}}^{\Lambda=0} = \mathcal{G}^{\Lambda=0}$)

$$G_\sigma(V_g) = \frac{e^2}{h}\, 4\Gamma_1^L\Gamma_N^R \left|\mathcal{G}^{\Lambda=0}_{\sigma;1,N}(0)\right|^2 . \tag{37}$$

The occupancy of dot j follows from integrating $\mathcal{G}^{\Lambda=0}_{j,j}(i\omega)$ over ω.

For the special case of equal nearest-neighbor inter-dot hoppings t, equal hybridizations $\Gamma_1^L = \pi|t_1^L|^2\rho_{\rm lead} = \Gamma_N^R = \pi|t_N^R|^2\rho_{\rm lead} = \Gamma/2$, equal local interactions U, and equal $\varepsilon_{j,\sigma} = V_g$, $G(V_g)$ at $T = 0$ was computed using NRG.[22,23] For this class of parameters the Hamiltonian has a high symmetry and the conductance is related to scattering phase shifts. The latter can be extracted from energies of the system which allowed to obtain results for a chain of up to four dots. In Fig. 8 we show a comparison of the NRG and fRG results (for G and the total dot occupancy $\langle n\rangle = \sum_{j,\sigma}\langle n_{j,\sigma}\rangle$) for $N = 4$, $U/\Gamma = 2\pi$, and $t/\Gamma = 1$. For gate voltages at which the four-site chain

is occupied by an odd number of electrons one finds a transmission peak of unitary height. Each corresponds to transport through mainly one of the four dot levels. For $U/\Gamma = 2\pi$ the plateau-like line shape of the individual resonances induced by the Kondo effect is only weakly developed. It becomes more pronounced if larger U/Γ are considered. The overlap of the resonances decreases for increasing t/Γ. For even N the width of all the resonances is almost equal and of order U/N. In a wide region around $V_g = 0$, $G(V_g)$ is small because close to half-filling of the chain charge fluctuations are strongly suppressed. For odd N, as in Fig. 9, half-filling corresponds to an odd number of electrons on the chain. This implies a wide plateau of unitary height around V_g due to the suppressed charge fluctuations (compare the solid lines in the upper $U/\Gamma = \pi$ and lower panel $U = 0$ of Fig. 9) and only the resonances away from $V_g = 0$ have width U/N.[22] The (spin-independent) transmission phase $\alpha_\sigma(V_g)$ and the total occupancy are related by $\langle n\rangle = 2\alpha_\sigma/\pi$.[23,68] Across every transmission resonance the phase continuously changes by π in analogy to the behavior of the phase at $U = 0$. Note that in contrast to the single-dot case α_σ is not restricted to the interval $[0, \pi]$.

For U/Γ smaller than the one of Fig. 8 the agreement between NRG and fRG further increases, e.g. for $N = 4$, $U/\Gamma = 1.67\pi$, and $t/\Gamma = 4.167$ both data sets are almost indistinguishable (for the NRG data see Fig. 5 of Ref. 23). We encounter serious deviations of the fRG data and NRG results if U/Γ is significantly increased (i.e. for $U/\Gamma = 8.33$; for NRG data see Fig. 4 of Ref. 23). In that case regions of gate voltages appear in which some of the components of the effective interaction become orders of magnitude larger than the initial U leading to a conductance that is too small. For these V_g it is no longer justified to neglect the frequency dependence of the 2-particle vertex and the higher-order vertices. In particular, this happens for V_g on-resonance and in addition for even N in the deep valley around $V_g = 0$. Indications of this breakdown of our approximation scheme for $U/\Gamma \gtrapprox 10$ can already be observed in the $V_g = 0$ valley, and the large $|V_g|$ resonances in Fig. 8: in these gate-voltage regimes our approximation significantly underestimates G.

In Fig. 9 we show how an increasing left-right asymmetry of the Γ_1^L and Γ_N^R affects the conductance for $N = 3$ for small to intermediate t/Γ. The parameters are $U/\Gamma = \pi$, with fixed $\Gamma = \Gamma_1^L + \Gamma_3^R$, and $t/\Gamma = 1$. For comparison in the lower panel we show the $U = 0$ case. With increasing asymmetry the height of the peaks decrease. While for fixed asymmetry the interaction leads to an enhancement of the outer two peaks, it suppresses the peak located around $V_g = 0$. Therefore, at $U > 0$ the central peak disappears quickly if Γ_1^L/Γ_3^R increases. It is important to note that with increasing asymmetry the gate voltage dependence of the total occupation $\langle n\rangle$ and the transmission phase α_σ (which are still related by $\langle n\rangle = 2\alpha_\sigma/\pi$) barely change. Thus these observables

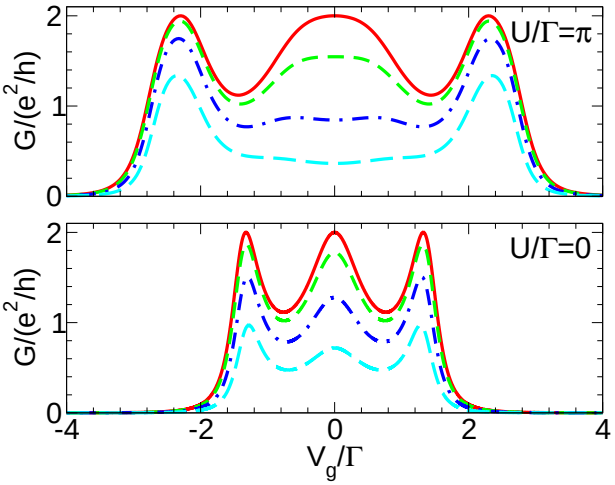

FIG. 9: (Color online) Gate Voltage dependence of the conductance G of a linear chain of $N = 3$ spin-degenerate dots with asymmetric coupling to the leads. The parameters are $U/\Gamma = \pi$ (upper panel), $U = 0$ (lower panel), $t/\Gamma = 1$, $\Gamma_1^L/\Gamma_3^R = 1$ (solid line), $\Gamma_1^L/\Gamma_3^R = 2$ (short dashed line), $\Gamma_1^L/\Gamma_3^R = 4$ (dashed-dotted line), and $\Gamma_1^L/\Gamma_3^R = 9$ (long dashed line). Note that here V_g is shown in units of Γ.

do not show any indication of the disappearance of the central resonance. The same holds for the (effective) dot level-positions of the chain obtained by diagonalizing the "effective Hamiltonian" at the end of the fRG flow (computed in the presence of the leads) after disconnecting the three sites from the leads. In particular, for all Γ_1^L/Γ_3^R studied one of the level energies (eigenenergies of the isolated chain at $\Lambda = 0$) goes through zero at $V_g = 0$. For levels which are not too strongly (sufficient separation of the resonances) and not too asymmetrically coupled to the leads one would thus expect a peak at $V_g = 0$ (see e.g. the $U = 0$ case). Surprisingly, during the fRG flow the effective asymmetry of the coupling to the outer two levels (as obtained from the eigenvectors of the isolated chain at $\Lambda = 0$) is reduced compared to the initial value, while the asymmetry of the central level is significantly increased by the presence of the interaction. Furthermore, the sum of the effective couplings of the central level to the left and right leads is increased which implies that the level is broadened. The combined effect of the asymmetry and broadening explains the vanishing of the central peak. For increasing peak separation, that is for increasing t/Γ, the central resonance becomes more robust against a left-right asymmetry.

The above observation might be important for the interpretation of future experiments on linear chains of quantum dots because asymmetric dot-lead couplings are generic in realistic dot systems. As shown, such an asymmetry might lead to a two peak structure although a chain of three sites is studied.

VI. SIDE-COUPLED DOUBLE DOTS

The side-coupled double dot of Fig. 1 D shows a very interesting low-energy physics. Close to half-filling it is either dominated by a two-stage Kondo effect for small $t_{1,2}$ or the formation of a local "molecular" spin-singlet between the electrons on the two dots for large $t_{1,2}$. Both regimes can be distinguished by the temperature dependence of the $G(V_g)$ curves as is nicely discussed in Ref. 28 (see also Ref. 29) based on NRG data. In the two-stage Kondo effect, first at high energies the spin of the embedded dot gets screened at the Kondo scale T_K^0 of the system with $t_{1,2} = 0$. In the second stage the heavy quasi-particles screen the spin on the side-coupled dot at a much lower scale T_0.

The $U = 0$ projected "effective Hamiltonian" for spin direction σ reads (in the wide-band limit)

$$h_\sigma(i\omega) = \begin{pmatrix} \varepsilon_{1,\sigma} - i(\Gamma_1^L + \Gamma_1^R)\,\mathrm{sgn}(\omega) & -t_{1,2} \\ -t_{1,2} & \varepsilon_{2,\sigma} \end{pmatrix} . \quad (38)$$

As for the linear chain of dots the projected noninteracting propagator $\mathcal{G}_0(i\omega)$ entering the flow equations (19) and (20) follows by the matrix inversion Eq. (36). Starting out with a local interaction U (and maybe a nearest-neighbor density-density interaction U') all two-particle interactions not excluded by symmetries are generated (see above). Also in the self-energy matrix all four matrix elements flow, that is, both the level positions and the inter-dot hopping are renormalized. As for the single dot we can use Eq. (29) to compute the conductance from the spectral weight of the embedded dot with $j = 1$ taken at $\Lambda = 0$.[28]

In Figs. 10 and 11 we compare fRG results for $G(V_g)$ to NRG data. Two different parameter sets with purely local interaction U, $\Gamma_1^L = \Gamma_1^R = \Gamma/2$, and $\varepsilon_{1,\sigma} = \varepsilon_{2,\sigma} = V_g$ are used. In Fig. 10 the parameters are in the spin-singlet regime: $U/\Gamma = 8$, $t_{1,2}/\Gamma = 4$.[28] The fRG and NRG data agree well. From the gate voltage dependence of the many-body eigenvalues of the double dot system without the leads[29] it becomes clear that each of the plateau-like resonances centered around $\pm V_g^p$ can be understood as the resonance in the single dot case, with the difference that the approximate width of the two peaks is $\Delta = U/2 + 2t_{1,2}\left[1 - \sqrt{1 + (U/4t_{1,2})^2}\right]$ instead of U. Around $V_g = 0$ both dots are half-filled and a local spin-singlet is formed leading to a suppression of the conductance. The parameters $U/\Gamma = 2$ and $t_{1,2}/\Gamma = 0.2$ of Fig. 11 are taken from the two-stage Kondo regime.[28] As U/Γ is moderate the first stage of the Kondo effect is not well pronounced which explains that the conductance away from half-filling (that is for $|V_g| \geq U/2$) vanishes only slowly with increasing $|V_g|$. For these gate voltages the fRG and NRG data are almost indistinguishable. The second stage of the Kondo effect generates a dip at $\omega = 0$ in the spectral function of dot $j = 1$ at half filling,[28] that leads to the suppression of G near $V_g = 0$. For small $t_{1,2}$ the scale $U/t_{1,2}^2$ relevant in the second stage of the Kondo effect becomes very large and, not surprisingly, our approximation deviates quantitatively (not qualitatively) from the NRG data for $|V_g| \leq U/2$. For these gate voltages some of the flowing interactions become large and our truncation scheme is questionable. Within our approximation the parameter regime of very large $U/t_{1,2}^2$, in which in addition to the two-stage Kondo effect a Fano-like feature in $G(V_g)$ was observed,[29] is out of reach.

In Figs. 10 and 11, in addition to G we show the dot oc-

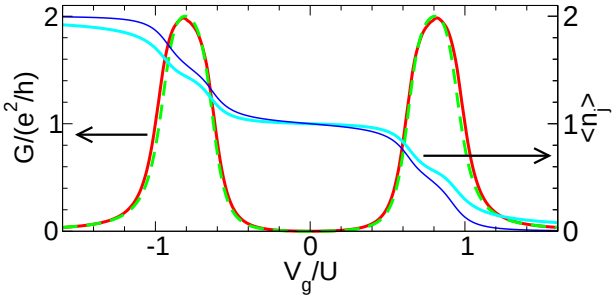

FIG. 10: (Color online) Gate Voltage dependence of the total conductance G and total occupancies $\langle n_j \rangle$ of a spin-degenerate side-coupled double-dot system (see Fig. 1 D) with $U/\Gamma = 8$ and $t_{1,2}/\Gamma = 4$. Solid line with left y-axis: NRG data for G from Ref. 28. Dashed line with left y-axis: fRG approximation of G with flow of vertex. Thick solid line with right y-axis: fRG approximation of $\langle n_1 \rangle$ (embedded dot). Thin solid line with right y-axis: fRG approximation of $\langle n_2 \rangle$ (attached dot).

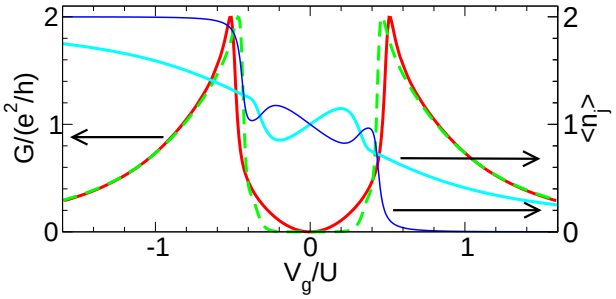

FIG. 11: (Color online) As in Fig. 10 but for $U/\Gamma = 2$ and $t_{1,2}/\Gamma = 0.2$.

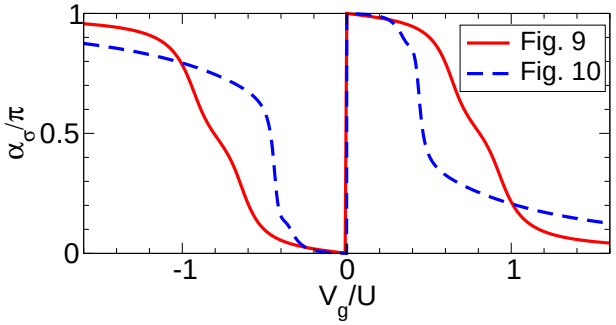

FIG. 12: (Color online) Gate Voltage dependence of the (spin-independent) transmission phase α_σ for the two parameter sets of Figs. 10 and 11.

cupancies $\langle n_j \rangle$, with $n_j = n_{j,\uparrow} + n_{j,\downarrow}$, computed by fRG. Because of the large inter-dot hopping in Fig. 10 the occupancies behave similarly for all V_g. For small $t_{1,2}$ (Fig. 11) the side-coupled dot $j = 2$ is coupled very weakly to the leads and the particle number of this dot changes very abruptly across the transmission resonances. Close to $V_g = 0$ the occupancies $\langle n_j \rangle$ depend non-monotonically on V_g. This follows from an interaction-induced non-monotonicity of the effective level positions. Similar behavior was observed in a spin-polarized parallel double-dot model.[33,69,70] In contrast the total dot charge $\langle n \rangle = \langle n_1 \rangle + \langle n_2 \rangle$ is monotonic. Similar to the single-dot case it is directly related to the conductance[28]

$$G/(e^2/h) = 2\sin^2\left(\langle n \rangle \pi/2\right). \tag{39}$$

The (spin-independent) transmission phase α_σ for the parameter sets of Figs. 10 and 11 is shown in Fig. 12. Experimentally this phase is accessible if the side-coupled double dot is placed in one arm of a "two-path" Aharonov-Bohm interferometer and the current oscillations as a function of a magnetic flux enclosed by the two arms are measured. Such measurements were already performed for single multi-level dots.[34] Across a transmission resonance the phase continuously changes by π. Associated to $G(V_g = 0) = 0$ is a phase jump of π. From α_σ the conductance can be computed as $G/(e^2/h) = 2\sin^2\alpha_\sigma$. Note that this relation together with Eq. (39) only implies $\alpha_\sigma = (\langle n_\sigma \rangle + m)\,\pi$, with $m \in \mathbb{Z}$ and the observed phase jumps by π are not excluded. The weak shoulder at $\alpha_\sigma \approx \pi/2$ for the parameters of Fig. 10 is related to the Kondo effect and develops into a plateau if U/Γ is increased.

From the $\mathcal{H} = 0$ conductance curves the two regimes (local spin-singlet and two-stage Kondo) cannot be distinguished unambiguously. In particular, in both cases G is suppressed very strongly close to half-filling. The $G(V_g)$ curves in the two regimes change quite differently in the presence of a magnetic field that lifts the spin-degeneracy of both levels: $\varepsilon_{1,\uparrow} = \varepsilon_{2,\uparrow} = V_g - \mathcal{H}/2$, $\varepsilon_{1,\downarrow} = \varepsilon_{2,\downarrow} = V_g + \mathcal{H}/2$. As for the single dot case studying the magnetic field dependence also enables us to define Kondo temperatures. For the two parameter sets of Figs. 10 and 11 $G(V_g)$ for different $\mathcal{H}$ is shown in Figs. 13 and 14. In the two-stage Kondo regime we define a scale T_K^0 for the first stage of the Kondo effect considering the single dot case, i.e. setting $t_{1,2} = 0$. For the parameters of Fig. 14 we obtain $T_K^0/\Gamma = 1.16$ in good agreement with the NRG estimate $T_K^0/\Gamma = 1$.[28] Because of its very small energy scale $T_0 \ll T_K^0$ the second stage of the Kondo effect gets destroyed already by a tiny magnetic field $\mathcal{H} \ll T_K^0$ and the local minimum of G at half-filling evolves into a maximum as shown in Fig. 14. We define T_0 by the magnetic field required to obtain $G(U, V_g = 0, \mathcal{H} = T_0) = e^2/h$. For the parameters of Fig. 14 this leads to $T_0/\Gamma = 0.003$. For larger $t_{1,2}$ (spin-singlet regime), as shown in Fig. 13, the spin-singlet is the ground state up to moderate $\mathcal{H}$ and $V_g = 0$ remains a minimum. The magnetic field dependence of

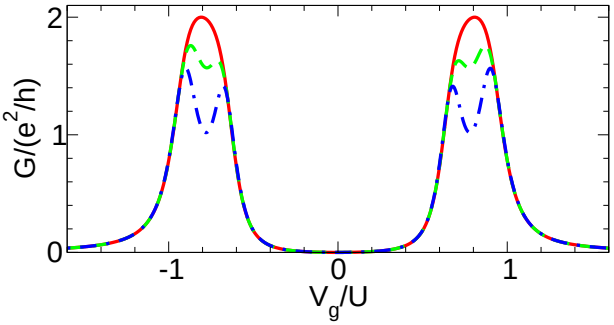

FIG. 13: (Color online) Gate Voltage dependence of the total conductance G for the parameters of Fig. 10 and different magnetic fields $\mathcal{H} = 0$ (solid line), $\mathcal{H} = 0.065\Gamma = 0.5T_K$ (dashed line), $\mathcal{H} = 0.13\Gamma = T_K$ (dashed-dotted line).

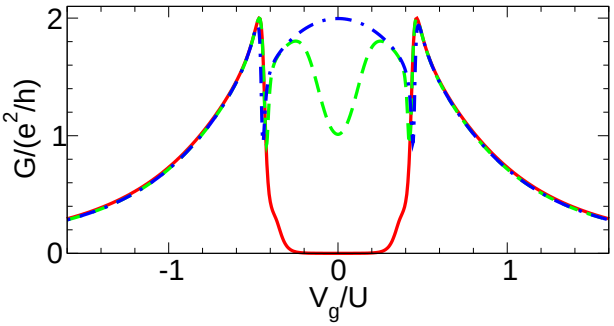

FIG. 14: (Color online) Gate Voltage dependence of the total conductance G for the parameters of Fig. 11 and different magnetic fields $\mathcal{H} = 0$ (solid line), $\mathcal{H} = 0.003\Gamma = T^0 = 0.0026T_K^0$ (dashed line), $\mathcal{H} = 0.03\Gamma = 10T^0 = 0.026T_K^0$ (dashed-dotted line).

the two resonances is similar to the single dot case. In this parameter regime it is meaningful to define a Kondo temperature T_K by $G(U, V_g = \pm V_g^p, \mathcal{H} = T_K) = e^2/h$. For the parameters of Fig. 13 we obtain $T_K/\Gamma = 0.13$, which is close to the NRG result $T_K/\Gamma = 0.156$.[28] In both parameter regimes the evolution of $G(V_g)$ with $\mathcal{H}$ is similar to the one with T discussed in Ref. 28.

For the present setup we also studied the role of (a) asymmetric dot-lead couplings $\Gamma_1^L \neq \Gamma_1^R$, (b) asymmetric local interactions $U_{1,1}^{\uparrow,\downarrow} \neq U_{2,2}^{\uparrow,\downarrow}$, and (c) a nearest-neighbor interaction $U_{j,\bar{j}}^{\sigma,\sigma'}$, with $\bar{j}$ denoting the complement of j. In case (a) the overall height of G decreases with increasing asymmetry while the line shape remains invariant similar to the case of a single dot.[64] Asymmetric local interactions and nearest-neighbor interactions only lead to quantitative changes but no new physics.

VII. PARALLEL DOUBLE DOTS

As our most complex example we finally study the parallel double dot of Fig. 1 E. The large number of parameters allows for a variety of different regimes and we here refrain from giving a complete account of the physics of

this setup. Instead, we focus on a few cases to exemplify that our approximation scheme can be used to uncover interesting effects. A more detailed discussion will be given in an upcoming publication. We here only consider the case without an inter-dot hopping. If present initially such a term can always be tuned away by a basis transformation on bonding and anti-bonding dot states. Note that in the noninteracting case the double dot can equally be viewed as a single two-level dot. Including the interaction both cases might be distinguished by the choice of non-vanishing matrix elements (see below). Correlated multi-level dots have recently attracted much interested in connection with the puzzling observation of "universal" phase lapses in a series of measurements of the transmission phase through quantum dots.[34] The conductance for the present setup with full spin polarization and small level detuning was earlier studied using the simplest fRG-based approximation scheme (considering only the flow of the self-energy) and NRG. In the absence of spin-Kondo physics the inter-dot (inter-level) interaction leads to novel correlation-induced resonances located exponentially (in U) close to $V_g = 0$.[33]

The noninteracting projected "effective Hamiltonian" of the present setup is given by

$$h_\sigma(i\omega) = \begin{pmatrix} \varepsilon_{1,\sigma} - i\Gamma_1 \,\mathrm{sgn}(\omega) & -i\gamma \,\mathrm{sgn}(\omega) \\ -i\gamma^* \,\mathrm{sgn}(\omega) & \varepsilon_{2,\sigma} - i\Gamma_2 \,\mathrm{sgn}(\omega) \end{pmatrix} \quad (40)$$

with

$$\Gamma_j = \sum_l \Gamma_j^l \,, \qquad \gamma = \sqrt{\Gamma_1^L \Gamma_2^L} + e^{i\phi}\sqrt{\Gamma_1^R \Gamma_2^R} \,. \quad (41)$$

We furthermore define

$$\Gamma = \sum_j \Gamma_j = \sum_j \sum_l \Gamma_j^l \,. \quad (42)$$

Here ϕ denotes a magnetic flux that goes through the ring geometry. If the system is viewed as a single two-level dot, ϕ is restricted to 0 and π, on which we will focus in the following. We denote the relative sign of the hopping matrix elements t_j^l by $s = e^{i\phi} = \pm 1$. The noninteracting propagator $\mathcal{G}_0(i\omega)$ follows by the matrix inversion Eq. (36). For generic parameters during the fRG flow Eqs. (19) and (20) the level positions are renormalized and a (real) direct inter-dot hopping is generated. Applying the projection technique Eq. (10) the conductance can be computed from the matrix elements of the projected Green function at $\Lambda = 0$

$$G_\sigma(V_g) = 4\,\frac{e^2}{h}\,\left|\sqrt{\Gamma_1^L\Gamma_1^R}\mathcal{G}^{\Lambda=0}_{\sigma;1,1}(0) + \sqrt{\Gamma_2^L\Gamma_1^R}\mathcal{G}^{\Lambda=0}_{\sigma;1,2}(0) + s\sqrt{\Gamma_1^L\Gamma_2^R}\mathcal{G}^{\Lambda=0}_{\sigma;2,1}(0) + s\sqrt{\Gamma_2^L\Gamma_2^R}\mathcal{G}^{\Lambda=0}_{\sigma;2,2}(0)\right|^2 \,. \quad (43)$$

The large number of parameters make it essential to analyze the conductance for the noninteracting case before considering the effect of two-particle interactions. A closed expression for $G_\sigma(V_g)$ at $U^{\sigma,\sigma'}_{j,j'} = 0$ can be obtained from Eq. (43) by replacing $\mathcal{G}^{\Lambda=0}(0)$ by $\mathcal{G}_0(0)$

$$G_\sigma(V_g) = \frac{e^2}{h}\,\frac{4\left[\Gamma_1^L\Gamma_1^R\varepsilon_{2,\sigma}^2 + \Gamma_2^L\Gamma_2^R\varepsilon_{1,\sigma}^2 + 2s\sqrt{\Gamma_1^L\Gamma_1^R\Gamma_2^L\Gamma_2^R}\varepsilon_{1,\sigma}\varepsilon_{2,\sigma}\right]}{\left[\Gamma_1^L\Gamma_2^R + \Gamma_2^L\Gamma_1^R - 2s\sqrt{\Gamma_1^L\Gamma_1^R\Gamma_2^L\Gamma_2^R} - \varepsilon_{1,\sigma}\varepsilon_{2,\sigma}\right]^2 + \left[\varepsilon_{1,\sigma}\Gamma_2 + \varepsilon_{2,\sigma}\Gamma_1\right]^2} \,. \quad (44)$$

We here focus on the spin-degenerate case with $\mathcal{H} = 0$. For generic level-lead couplings[33] Γ_j^l and $\delta = \varepsilon_{2,\sigma} - \varepsilon_{1,\sigma} \geq 0$ the gate voltage dependence ($\varepsilon_{1/2,\sigma} = \mp\delta/2 + V_g$) of Eq. (44) is characterized by two peaks (of height $\leq e^2/h$) and a conductance zero. The latter follows from perfect destructive interference at a particular V_g. Associated to the zero is a jump of the transmission phase by π. Further details of $G_\sigma(V_g)$ depend on s. For $s = +1$ the conductance zero is located between the two conductance peaks for all δ. For $\delta \to 0$ the peak positions depend on the asymmetry of the Γ_j^l and the separation of the peaks is small if the Γ_j^l are almost equal. For equal Γ_j^l and $\delta = 0$ the zero disappears. For $s = -1$ and fixed Γ_j^l the position of the conductance zero with respect to the peaks depends on δ. For $\delta \to 0$ it is located between the two conductance peaks, while it lies outside for large δ. In the crossover regime between these limiting cases one of the peaks vanishes, while the other becomes broader and splits up into two resonances separated by a minimum with non-vanishing conductance. For Γ_j^l with 1-2 symmetry and $\delta \to 0$ the conductance vanishes for all V_g as the model can be mapped onto a model with two levels, each one only coupled to one of the leads. In this (and only this) case a pseudo-spin variable is conserved leading to an orbital Kondo effect if a nearest-neighbor interaction is added.[31,32] For fixed, asymmetric Γ_j^l and $\delta \to 0$ the separation of the two conductance peaks for $s = -1$ is much larger than for $s = +1$. For certain classes of

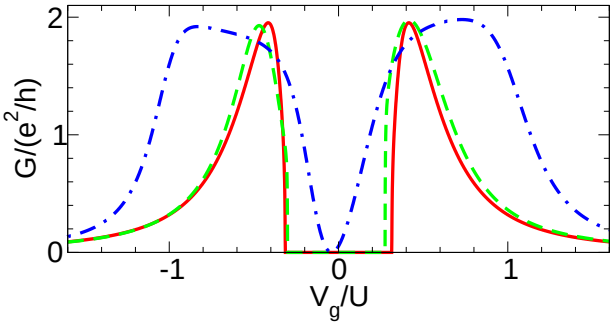

FIG. 15: (Color online) Gate Voltage dependence of the total conductance G of a parallel double dot (see Fig. 1 E) with generic Γ_j^l, spin-degenerate levels, purely local interactions, and different level detunings δ. The parameters are $U/\Gamma = 4$, $\Gamma_1^L/\Gamma = 0.27$, $\Gamma_1^R/\Gamma = 0.33$, $\Gamma_2^L/\Gamma = 0.16$, $\Gamma_2^R/\Gamma = 0.24$, $s = 1$, $\delta/\Gamma = 0$ (solid line), $\delta/\Gamma = 1$ (dashed line), and $\delta/\Gamma = 5$ (dashed-dotted line).

parameters, some of them we mentioned already (e.g., equal Γ_j^l and $\delta = 0$; see Ref. 33 for details), $G(V_g)$ does not follow the behavior described above. Here, we do not investigate these special cases but focus on the generic behavior.

In Fig. 15 we show $G(V_g)$ for a generic set of Γ_j^l, $s = +1$, and different δ. We assume a purely local interaction U, which might experimentally be realized if the setup is implemented as two single-level dots of sufficient spatial separation. Close to half-filling the conductance is strongly suppressed. In particular this holds for small δ. We note that around $V_g = 0$ the flowing two-particle vertex becomes large which indicates that our approximation scheme becomes less accurate. Further down we return to this issue. For $\delta/\Gamma \leq 1$ the curves of Fig. 15 are similar to the one of Fig. 11 obtained for the side-coupled double dot with small inter-dot hopping $t_{1,2}$. We argue that this similarity follows from a relation between the two double-dot geometries which we investigate next.

Taking the even and odd linear combination of dot states the noninteracting side-coupled dot (index s) with $\left(t_1^L\right)_s$, $\left(t_1^R\right)_s$, $\left(t_{1,2}\right)_s$, and $\left(\varepsilon_{j,\sigma}\right)_s = V_g$ can be mapped on the parallel dot with parameters

$$\begin{aligned} t_1^L &= \left(t_1^L\right)_s/\sqrt{2}\,, \quad t_1^R = \left(t_2^R\right)_s/\sqrt{2}\,, \\ t_2^L &= \left(t_1^L\right)_s/\sqrt{2}\,, \quad t_2^R = \left(t_2^R\right)_s/\sqrt{2}\,, \\ \varepsilon_{1,\sigma} &= V_g - \left(t_{1,2}\right)_s\,, \quad \varepsilon_{2,\sigma} = V_g + \left(t_{1,2}\right)_s\,, \end{aligned} \tag{45}$$

that is, $\delta = 2\left(t_{1,2}\right)_s$. Note that small $\left(t_{1,2}\right)_s$ correspond to small δ. This subset of the large parameter space of the parallel double dot is characterized by a 1-2 symmetry of the hoppings and $s = 1$. A local interaction of the side-coupled dot

$$U_s \sum_j n_{j,\uparrow}^s n_{j,\downarrow}^s\,. \tag{46}$$

maps onto

$$\begin{aligned} &\frac{U_s}{2}\left(\sum_j n_{j,\uparrow}n_{j,\downarrow} + n_{1,\uparrow}n_{2,\downarrow} + n_{1,\downarrow}n_{2,\uparrow}\right) \\ &+\frac{U_s}{2}\left(d_{2,\uparrow}^\dagger d_{1,\uparrow} d_{2,\downarrow}^\dagger d_{1,\downarrow} + d_{2,\uparrow}^\dagger d_{1,\uparrow} d_{1,\downarrow}^\dagger d_{2,\downarrow}\right. \\ &\left.+d_{1,\uparrow}^\dagger d_{2,\uparrow} d_{2,\downarrow}^\dagger d_{1,\downarrow} + d_{1,\uparrow}^\dagger d_{2,\uparrow} d_{1,\downarrow}^\dagger d_{2,\downarrow}\right) \end{aligned} \tag{47}$$

for the parallel double dot. Besides the usual density interactions also correlated hoppings are generated by this transformation.[71]

These considerations show that the cases studied in Figs. 11 and 15 (for $\delta/\Gamma \leq 1$) are related but not completely equivalent as in Fig. 15 we only considered a local interaction and no 1-2 symmetry of the Γ_j^l. Slowly increasing the amplitudes of the additional interactions Eq. (47) and tuning the Γ_j^l towards 1-2 symmetry we convinced ourselves that both the symmetry and the additional interactions do not play an essential role and the results for the parallel double dot with $\delta/\Gamma \leq 1$ of Fig. 15 can be interpreted as for the side-coupled double dot in the two-stage Kondo regime. The strong suppression of the conductance of the parallel double dot around half-filling for small δ then follows from the second stage of the Kondo effect. From the side-coupled dot we already know that our approximation scheme overestimates this suppression and we believe that the same holds for the present geometry. Note that for $\delta = 0$, $G(V_g)$ is symmetric around $V_g = 0$ as the Hamiltonian is symmetric under a particle-hole transformation if in addition $V_g \to -V_g$. Despite the asymmetry of the Γ_j^l the two resonances have almost unitary height. For small δ the occupancies of the two levels are similar, sharply change across the two resonances, and display a plateau at 1 close to $V_g = 0$. The transmission phase increases by π across the resonances and jumps by π in between the peaks.

For large δ, $G(V_g)$ in Fig. 15 can be understood from the eigenvalues of the many-body dot Hamiltonian without the leads, in analogy to the limit of large $\left(t_{1,2}\right)_s$ for the side-coupled dot. Each of the resonances then corresponds to a single-level resonance, as discussed in Sec. IV. Because of the asymmetry of the Γ_j^l, the conductance does not reach the unitary limit and the two resonances have different line shape. Associated with the resonances is a change of one of the $\langle n_j\rangle$ from 2 to 0 (change of the phase from 0 to π) and a plateau at 1 (at $\pi/2$ for the phase) within the resonance. For the Γ_j^l of Fig. 15, $\langle n_2\rangle$ changes across the peak at $V_g < 0$ and $\langle n_1\rangle$ across the one at $V_g > 0$. The plateaus in $\langle n_j\rangle$ and α_σ are due to the Kondo effect that is active at each of the resonances. At the conductance zero between the conductance peaks the transmission phase jumps by π.

Scanning the parameter space with fixed $s = +1$ we encountered an interesting correlation effect for a model with almost equal local and nearest-neighbor density interactions, small δ, and generic Γ_j^l. It is exemplified in Fig. 16. In the lower panel of Fig. 16 we show $G(V_g)$ for

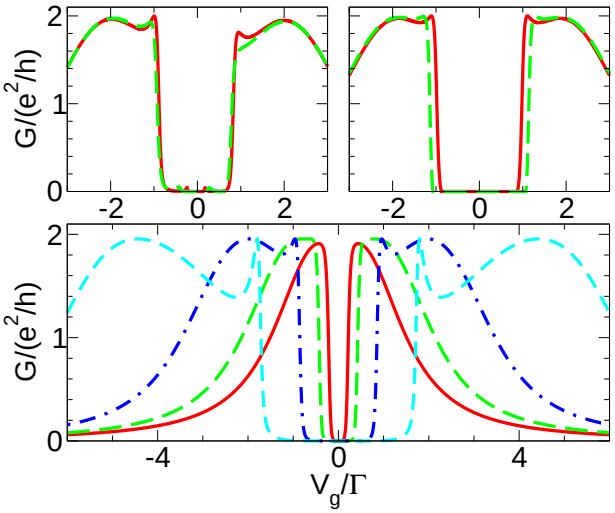

FIG. 16: (Color online) Gate Voltage dependence of the total conductance G of a parallel double dot with generic Γ_j^l, spin-degenerate levels, and (almost) equal local and nearest-neighbor density interactions. The parameters are $\Gamma_1^L/\Gamma = 0.5$, $\Gamma_1^R/\Gamma = 0.25$, $\Gamma_2^L/\Gamma = 0.07$, $\Gamma_2^R/\Gamma = 0.18$, and $s = 1$. *Lower panel:* Equal level positions on both dots $\delta = 0$ and equal local and nearest-neighbor interactions U with $U/\Gamma = 0.5$, (solid line) 1 (long dashed line), 2 (dashed-dotted line), and 4 (short dashed line). *Upper left panel:* Stability of the novel resonances for non-vanishing level detuning δ at $U/\Gamma = 2$. $\delta/\Gamma = 0.03$ (solid line) and $\delta/\Gamma = 0.07$ (dashed line). *Upper right panel:* Stability of the novel resonances for asymmetric interactions at $\delta = 0$. $U_{1,1}^{\sigma,\bar\sigma}/\Gamma = 1.9$, $U_{2,2}^{\sigma,\bar\sigma}/\Gamma = 2.1$, $U_{j,\bar j}^{\sigma,\sigma}/\Gamma = 1.8$, $U_{j,\bar j}^{\sigma,\bar\sigma}/\Gamma = 2$ (solid line) and $U_{1,1}^{\sigma,\bar\sigma}/\Gamma = 1.8$, $U_{2,2}^{\sigma,\bar\sigma}/\Gamma = 2.2$, $U_{j,\bar j}^{\sigma,\sigma}/\Gamma = 1.7$, $U_{j,\bar j}^{\sigma,\bar\sigma}/\Gamma = 2.2$ (dashed line). Note that here V_g is shown in units of Γ.

$\delta = 0$ and $U_{j,j'}^{\sigma,\sigma'} = U(1-\delta_{j,j'}\delta_{\sigma,\sigma'})$. Increasing U, the peak conductance increases, the two maxima become flat, and for U larger than a Γ_j^l dependent critical $U_c(\{\Gamma_j^l\})$ both split up into two peaks. For $U > U_c$ the height of all four resonances is equal and U independent. The two outermost peaks are located at $V_g \approx \pm U$ and the inner two at $V_g \approx \pm U/2$. This scenario is quite similar to the appearance of additional correlation induced resonances in a spin-polarized model of a parallel double dot with nearest-neighbor interaction as discussed in Ref. 33. The novel resonances follow from the combined presence of correlations and quantum interference. In the upper panels of Fig. 16 we show that the effect is robust against a small level detuning δ and a small asymmetry of the $U_{j,j'}^{\sigma,\sigma'}$. It will be further investigated in an upcoming publication. One can expect that in experimentally realized single two-level dots the inter- and intra-dot density interactions are indeed (almost) equal and the additional resonances should thus be observable in such systems.

We next study the case $s = -1$. As for $s = +1$ above we first investigate systems with purely local interactions (two well-separated single-level dots) and further down a situation with (almost) equal local and nearest-neighbor interactions (a single two-level dot).

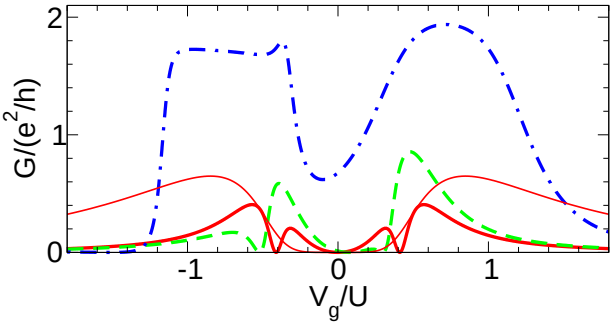

FIG. 17: (Color online) Gate Voltage dependence of the total conductance G of a parallel double dot with generic Γ_j^l, spin-degenerate levels, purely local interactions, and different level detunings δ. The parameters are $U/\Gamma = 4$ (thick lines), $U/\Gamma = 1$ (thin line) $\Gamma_1^L/\Gamma = 0.5$, $\Gamma_1^R/\Gamma = 0.35$, $\Gamma_2^L/\Gamma = 0.05$, $\Gamma_2^R/\Gamma = 0.1$, $s = -1$, $\delta/\Gamma = 0$ (solid line), $\delta/\Gamma = 0.6$ (dashed line), and $\delta/\Gamma = 6$ (dashed-dotted line).

In Fig. 17 we show $G(V_g)$ for $s = -1$, generic Γ_j^l, a purely local interaction, and different δ. Without loss of generality we consider Γ_j^l with a fairly large 1-2 asymmetry. Otherwise the conductance at small δ is very small. This follows from the fact that for 1-2 symmetric Γ_j^l and $\delta = 0$, $G(V_g) = 0$ for all V_g, as discussed above. The thin solid curve shows the case with $\delta = 0$ and $U/\Gamma = 1$, that is qualitatively similar to the $U = 0$ case. Increasing U (at $\delta = 0$) each of the two peaks splits up into two with a conductance zero in between. In Fig. 17 this is shown as the thick solid line for $U/\Gamma = 4$. The dashed and dashed-dotted lines show how the conductance evolves with increasing level detuning δ at fixed $U/\Gamma = 4$. The conductance zeros either vanish or are pushed towards larger $|V_g|$. The overall conductance increases. For large δ the two remaining resonances can be understood as in the single-dot, single-level case. Across the resonance centered around $-\delta/2$ ($+\delta/2$) level 2 (1) gets filled. As the Γ_2^l are small the effective interaction $U/(\Gamma_2^L + \Gamma_2^R)$ relevant for the Kondo effect is large and the resonance at $V_g < 0$ has a well-developed plateau-like line shape. These results can most easily be understood by making contact with the case of left-right symmetric Γ_j^l. In this case the off-diagonal element γ [see Eq. (41)] of the non-interacting "effective Hamiltonian" (40) vanishes. As the interaction is purely local no such term (that is a hopping between $j = 1$ and $j = 2$) is generated during the fRG flow and the double-dot problem separates into two single-dot problems. In particular, $\mathcal{G}_{\sigma;1,2}^{\Lambda=0}$ vanishes and the conductance Eq. (43) is given by the sum of two single-level Green functions. Breaking of the left-right symmetry leads to a small initial off-diagonal element, that stays small during the fRG flow. For that reason also the results of Fig. 17 can be understood from the single-level case. E.g., this explains the position $V_g \approx \pm\delta/2$ of the resonances at large δ. A more detailed discussion will be given elsewhere.

In Fig. 18 we show how the four-peak structure obtained for a sufficiently large local interaction U at $\delta = 0$

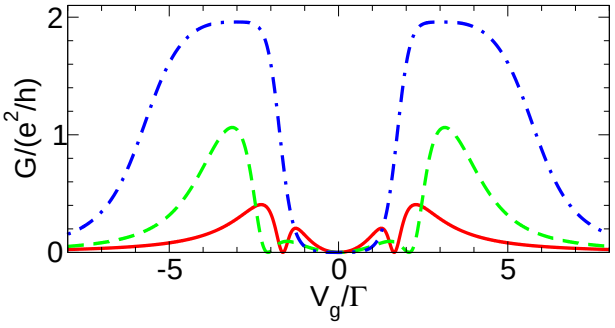

FIG. 18: (Color online) Gate Voltage dependence of the total conductance G of a parallel double dot with generic Γ_j^l, $s = -1$, spin-degenerate levels, $\delta = 0$, local interaction $U/\Gamma = 4$, and different nearest-neighbor interactions $U' = 0$ (solid line), $U'/\Gamma = 2$ (dashed line), and $U'/\Gamma = 4$ (dashed-dotted line). The Γ_j^l are as in Fig. 17. Note that here V_g is shown in units of Γ.

and $s = -1$ disappears in the presence of a nearest-neighbor interaction U' (single two-level dot). Starting out with four peaks of almost equal height at $U' = 0$, for increasing U' the two outermost peaks gain weight, while the inner two peaks lose weight. At $U' = U$ only two resonances remain.

VIII. SUMMARY AND OUTLOOK

In the present paper we have introduced a novel approximate method to study electronic transport through systems of quantum dots with local Coulomb correlations. Our fRG-based approximation scheme results in a set of coupled differential flow equations for the interaction-dependent effective level positions and inter-level hoppings as well as the interaction matrix elements. We have solved the flow equations for a variety of dot systems and computed the linear conductance, the transmission phase, and level occupancies.

For several setups and parameter sets we compared our results to existing exact Bethe ansatz and high precision NRG data. For a single dot the agreement is excellent up to the largest Coulomb interaction for which Bethe ansatz or NRG data are available. In particular, we showed analytically that our approach covers the signatures of the Kondo effect. The method performs very well also in the presence of a magnetic field lifting the spin degeneracy and in case of an additional direct transmission channel between the leads (Fano effect). The field dependence of $G(V_g)$ allows us to extract the Kondo temperature that compares well to the exact expression. For linear chains of dots (short Hubbard chains) we found quantitative agreement with NRG data up to fairly large interactions. We studied the effect of a left-right asymmetry of the level-lead couplings that leads to the surprising vanishing of resonances if sufficiently large. For a side-coupled double-dot system we demonstrated that our method can be used to describe both the "molecular" spin-singlet regime at large inter-dot hoppings $t_{1,2}$ and the two-stage Kondo regime at small $t_{1,2}$. For not too small $t_{1,2}$ and too large interactions the approximate results agree well with NRG data. Our approximation scheme becomes questionable if $U/t_{1,2}^2$ becomes too large. We showed that the occupancies in the two-stage Kondo regime depend non-monotonically of the gate voltage. At $T = 0$ the different physics of the two regimes can be probed by a magnetic field lifting the spin degeneracy. Finally we demonstrated that the physics of a parallel single-level double dot (single two-level dot) is very rich. For a certain parameter regime we showed that $G(V_g)$ can be understood in analogy to the side-coupled double dot. For other classes of parameters we surprisingly found additional resonance peaks that should be observable experimentally in existing double-dot setups (two-level dots). A more complete analysis of the transport properties of the parallel double dot (single two-level dot) will be given in an upcoming publication.

The present paper shows that our approximation scheme is a simple-to-implement and reliable method to study transport through dot systems with a significant number of interacting degrees of freedom. It can be used to study setups that due to their complexity cannot be tackled by NRG. Even in problems that can be investigated by NRG our method is far superior in terms of the numerical effort required, e.g. enabling efficient analysis of parameter dependencies.

In summary, we have shown that the fRG based approximation scheme is a very promising tool to investigate the interesting physics of quantum dot systems resulting from Coulomb correlations (Kondo effect) and quantum interference.

Acknowledgments

We are grateful to P. Cornaglia, T. Costi, J. von Delft, W. Hofstetter, and A. Oguri for providing their NRG and Bethe ansatz data and thank S. Andergassen, J. von Delft, R. Hedden, W. Hofstetter, W. Metzner, Th. Pruschke, M. Reginatto, H. Schoeller, K. Schönhammer, and M. Weyrauch for valuable discussions. T.E. is grateful for support by a Feoder Lynen fellowship of the Alexander von Humboldt foundation and the Istituto Nazionale di Fisica della Materia–SMC–CNR. V.M. is grateful to the Deutsche Forschungsgemeinschaft (SFB 602) for support.

[1] *Mesoscopic Electron Transport*, edited by L.L. Sohn, L.P. Kouwenhoven, and G. Schön (Kluwer, Dordrecht, 1997).

[2] D. Loss and D.P. DiVincenzo, Phys. Rev. A **57**, 120 (1998); D. Loss and E.V. Sukhorukov, Phys. Rev. Lett. **84**, 1035 (2000).

[3] F. Marquardt and C. Bruder, Phys. Rev. B **68**, 195305 (2003).

[4] A.W. Holleitner, C.R. Decker, H. Qin, K. Eberl, and R.H. Blick, Phys. Rev. Lett. **87**, 256802 (2001); A. W. Holleitner, R.H. Blick, A.K. Hüttel, K. Eberl, and J.P. Kotthaus, Science **297**, 70 (2002).

[5] J.C. Chen, A.M. Chang, and M.R. Melloch, Phys. Rev. Lett. **92**, 176801 (2004).

[6] M. Sigrist, A. Fuhrer, T. Ihn, K. Ensslin, S.E. Ulloa, W. Wegschneider, and M. Bichler, Phys. Rev. Lett. **93**, 066802 (2004).

[7] A. W. Holleitner, A. Chudnovskiy, D. Pfannkuche, K. Eberl, and R.H. Blick, Phys. Rev. B **70**, 075204 (2004).

[8] J.R. Petta, A.C. Johnson, C.M. Marcus, M.P. Hanson, and A.C. Gossard, Phys. Rev. Lett. **93**, 186802 (2004).

[9] N.J. Craig, J.M. Taylor, E.A. Lester, C.M. Marcus, M.P. Hanson, and A.C. Gossard, Science **304**, 565 (2004).

[10] F.H.L. Koppens, J.A. Folk, J.M. Elzerman, R. Hanson, L.H. Willems van Beveren, I.T. Vink, H.P. Tranitz, W. Wegscheider, L.P. Kouwenhoven, and L.M.K. Vandersypen, Science **309**, 1346 (2005).

[11] J.R. Petta, A.C. Johnson, J.M. Taylor, E.A. Laird, A. Yacoby, M.D. Lukin, C.M. Marcus, M.P. Hanson, and A.C. Gossard, Science **309**, 2180 (2005).

[12] A.C. Johnson, J.R. Petta, J.M. Taylor, A. Yacoby, M.D. Lukin, C.M. Marcus, M.P. Hanson, and A.C. Gossard, Nature **435**, 925 (2005).

[13] A.C. Hewson, *The Kondo Problem to Heavy Fermions*, (Cambridge University Press, Cambridge, UK, 1993).

[14] L. Glazman and M. Raikh, JETP Lett. **47**, 452 (1988).

[15] T. Ng and P. Lee, Phys. Rev. Lett. **61**, 1768 (1988).

[16] D. Goldhaber-Gordon, H. Shtrikman, D. Mahalu, D. Abusch-Magder, U. Meirav, and M.A. Kastner, Nature **391**, 156 (1998).

[17] W. van der Wiel, S. De Franceschi, T. Fujisawa, J.M. Elzerman, S. Tarucha, and L.P. Kouwenhoven, Science **289**, 2105 (2000).

[18] L.P. Kouwenhoven and L. Glazman, Physics World, 33 (2001).

[19] A.M. Tsvelik and P.B. Wiegmann, Adv. Phys. **32**, 453 (1983).

[20] T.A. Costi, A.C. Hewson, and V. Zlatic, J. Phys.: Condens. Matter **6**, 2519 (1994).

[21] U. Gerland, J. von Delft, T.A. Costi, and Y. Oreg, Phys. Rev. Lett. **84**, 3710 (2000).

[22] A. Oguri and A.C. Hewson, J. Phys. Soc. Jpn. **74**, 988 (2005); A. Oguri, Y. Nisikawa, and A.C. Hewson, *ibid* **74**, 2554 (2005).

[23] Y. Nisikawa and A. Oguri, Phys. Rev. B **73**, 125108 (2006).

[24] R. Žitko, J. Bonča, A. Ramšak, and T. Rejec, Phys. Rev. B **73**, 153307 (2006).

[25] U. Fano, Phys. Rev. **124**, 1866 (1961).

[26] W. Hofstetter, J. König, and H. Schoeller, Phys. Rev. Lett. **87**, 156803 (2001).

[27] T.-S. Kim and S. Hershfield, Phys. Rev. B **63**, 245326 (2001).

[28] P.S. Cornaglia and D.R. Grempel, Phys. Rev. B **71**, 075305 (2005).

[29] R. Žitko and J. Bonča, Phys. Rev. B **73**, 035332 (2006).

[30] W. Izumida, O. Sakai, and Y. Shimizu, J. Phys. Soc. Jpn. **66**, 717 (1997).

[31] D. Boese, W. Hofstetter, and H. Schoeller, Phys. Rev. B **64**, 125309 (2001).

[32] D. Boese, W. Hofstetter, and H. Schoeller, Phys. Rev. B **66**, 125315 (2002).

[33] V. Meden and F. Marquardt, Phys. Rev. Lett. **96**, 146801 (2006).

[34] A. Yacoby, M. Heiblum, D. Mahalu, and H. Shtrikman, Phys. Rev. Lett. **74**, 4047 (1995); R. Schuster, E. Buks, M. Heiblum, D. Mahalu, V. Umansky, and H. Shtrikman, Nature **385**, 417 (1997); M. Avinun-Kalish, M. Heiblum, O. Zarchin, D. Mahalu, and V. Umansky, Nature **436**, 529 (2005).

[35] K.G. Wilson, Rev. Mod. Phys. **47**, 773 (1975).

[36] H.B. Krishnamurthy, J.W. Wilkins, and K.G. Wilson, Phys. Rev. B **21**, 1044 (1980).

[37] V. Kashcheyevs, A. Aharony, and O. Entin-Wohlman, Phys. Rev. B **73**, 125338 (2006).

[38] Y. Oreg and Y. Gefen, Phys. Rev. B **55**, 13726 (1997).

[39] H. Schoeller in *Low-Dimensional Systems*, ed. T. Brandes (Springer, 1999), p. 137.

[40] See C.A. Büsser, G.B. Martin, K.A. Al-Hassanieh, A. Moreo, and E. Dagotto, Phys. Rev. B **70**, 245303 (2004) and references therein.

[41] A. Oguri, cond-mat/0310139.

[42] M.E. Torio, K. Hallberg, A.H. Ceccatto, and C.R. Proetto, Phys. Rev. B **65**, 085302 (2002).

[43] G. Kotliar and A.E. Ruckenstein, Phys. Rev. Lett. **57**, 1362 (1986).

[44] B. Dong and X.L. Lei, J. Phys.: Condens. Matter **13**, 9245 (2001).

[45] J. Takahashi and S. Tasaki, cond-mat/0603337.

[46] B. Dong and X.L. Lei, Phys. Rev. B **63**, 235306 (2001).

[47] See Y. Tanaka and N. Kawakami, Phys. Rev. B **72**, 085304 (2005) and references therein.

[48] O. Gunnarsson and K. Schönhammer, Phys. Rev. B **31**, 4815 (1985).

[49] T. Rejec and A. Ramšak, Phys. Rev. B **68**, 035342 (2003).

[50] M. Salmhofer, *Renormalization*, (Springer, Berlin, 1998).

[51] D. Zanchi and H.J. Schulz, Phys. Rev. B **61**, 13609 (2000); C.J. Halboth and W. Metzner, *ibid* **61**, 7364 (2000); C. Honerkamp, M. Salmhofer, N. Furukawa, and T.M. Rice, *ibid* **63**, 035109 (2001).

[52] R. Hedden, V. Meden, Th. Pruschke, and K. Schönhammer, J. Phys.: Condens. Matter **16**, 5279 (2004).

[53] C. Honerkamp, D. Rohe, S. Andergassen, and T. Enss, Phys. Rev. B **70**, 235115 (2004).

[54] C. Wetterich, Phys. Lett. B **301**, 90 (1993).

[55] T.R. Morris, Int. J. Mod. Phys. A **9**, 2411 (1994).

[56] M. Salmhofer and C. Honerkamp, Prog. Theor. Phys. **105**, 1 (2001).

[57] S. Andergassen, T. Enss, and V. Meden, Phys. Rev. B **73** 153308 (2006).

[58] Note that in contrast to Eq. (2), Eq. (3) does not contain a minus sign. We here follow the convention of Ref. 26.

[59] For a review on the Landauer-Büttiker approach to transport see: S. Datta, *Electronic Transport in Mesoscopic Systems*, (Cambridge University Press, Cambridge, 1995).

[60] J.R. Taylor, *Scattering Theory*, (John Wiley and Sons, New York, 1972).

[61] A. Oguri, J. Phys. Soc. Jpn. **70**, 2666 (2001).

[62] J.W. Negele and H. Orland, *Quantum Many-Particle Physics*, (Addison-Wesley, Reading, 1988).

[63] V. Meden, lecture notes on the "Functional renormalization group",

http://www.theorie.physik.uni-goettingen.de/∼meden/funRG/

[64] Y. Meir and N.S. Wingreen, Phys. Rev. Lett. **68**, 2512 (1992).

[65] T. Enss, Ph.D. thesis, Universität Stuttgart 2005, URL: http://elib.uni-stuttgart.de/opus/volltexte/2005/2258, cond-mat/0504703.

[66] T.A. Costi, Phys. Rev. B **64**, 241310(R) (2001).

[67] Note that in Ref. 52 in addition to the scheme involving the single-scale propagator S^Λ a modified approximation is used. In the latter, S^Λ in the flow equation for Γ^Λ is replaced by $-\frac{\partial}{\partial\Lambda}\mathcal{G}^\Lambda$. We verified that for the truncation scheme used in the present publication this modification does not lead to any significant improvement of the results. This has to be contrasted to the truncation scheme of Ref. 52 involving frequency dependence in which the above replacement leads to much better agreement with NRG results.

[68] Note that the transmission phase α_σ is given by the sum of the phases δ_{even} and δ_{odd} defined in Ref. 23.

[69] M. Sindel, A. Silva, Y. Oreg, and J. von Delft, Phys. Rev. B **72**, 125316 (2005).

[70] J. König and Y. Gefen, Phys. Rev. B **71**, 201308(R) (2005).

[71] Note that Eq. (47) does not contain terms proportional to $n_{1,\sigma}n_{2,\sigma}$. If a nearest-neighbor interaction of strength U_s is added the interacting part of the side-coupled double-dot Hamiltonian reads $\frac{U_s}{2}\sum_{(j,\sigma)\neq(j',\sigma')} n^s_{j,\sigma}n^s_{j',\sigma'}$. This interaction is then invariant under the basis transformation onto the parallel double dot.[32]